Journal of Controlled Release 333 (2021) 298–315

Contents lists available at ScienceDirect

Journal of Controlled Release

journal homepage: www.elsevier.com/locate/jconrel

Artemether and lumefantrine dissolving microneedle patches with improved pharmacokinetic performance and antimalarial efficacy in mice infected with *Plasmodium yoelii*

Fabiana Volpe-Zanutto [a,b,c], Letícia Tiburcio Ferreira [d], Andi Dian Permana [b,e], Melissa Kirkby [b], Alejandro J. Paredes [b], Lalitkumar K. Vora [b], Amanda P. Bonfanti [c,f], Ives Charlie-Silva [g], Catarina Raposo [c], Mariana C. Figueiredo [c], Ilza M.O. Sousa [c], Andi Brisibe [h], Fabio Trindade Maranhão Costa [d], Ryan F. Donnelly [b,*], Mary Ann Foglio [c,*]

[a] *Graduate School of Bioscience and Technology of Bioactive products, Biology Institute, R. Monteiro Lobato, 255 - Cidade Universitária, Campinas - SP, 13083-862, University of Campinas, Brazil*
[b] *School of Pharmacy, Queen's University Belfast, Medical Biology Centre, 97 Lisburn Road, Belfast BT9 7BL, UK*
[c] *Faculty of Pharmaceutical Sciences, R. Cândido Portinari, 200 - Cidade Universitária, Campinas - SP, 13083-871, University of Campinas, Brazil*
[d] *Department of Genetics, Evolution, Microbiology & Immunology, Laboratory of Tropical Diseases - Prof Dr Luiz Jacintho da Silva, Institute of Biology, R. Carl Von Linaeus, 2-238 - Cidade Universitária, Campinas - SP, 13083-864, University of Campinas, Brazil*
[e] *Department of Pharmaceutics, Faculty of Pharmacy, Hasanuddin University, Makassar 90245, Indonesia*
[f] *Department of Funtional and Structural Biology, Biology Institute, R. Monteiro Lobato, 255 - Cidade Universitária, Campinas - SP, 13083-862, University of Campinas, Brazil*
[g] *Department of Pharmacology, Institute of Biomedical Sciences, Av. Prof. Lineu Prestes 1524, São Paulo, SP, 05508-900, University of São Paulo, Brazil*
[h] *University of Calabar, Calabar, Nigeria*

ARTICLE INFO

Keywords:
Dissolving microneedles
Nanosupensions
Artemether
Lumefantrine
Malaria
Plasmodium yoelii
Bioavailability

ABSTRACT

Malaria affects more than 200 million people annually around the world, killing a child every 2 min. Artemether (ART) and lumefantrine (LUM) are the gold standard choice to treat uncomplicated *Plasmodium falciparum* malaria; however, they are hydrophobic compounds with low oral bioavailability. Microneedle (MN) arrays consist of micron-sized needles on one side of a supporting base and have the ability to bypass the skin's *stratum corneum* barrier in a minimally invasive way, creating temporary channels through which drugs can diffuse, including those with poor water solubility. Herein, we report the development of dissolving MNs (DMNs) containing ART (MN-ART) and LUM (MN-LUM) as an alternative treatment regimen for malaria in low-resource settings. To incorporate the drugs into the MNs, nanosuspensions (NSs) for both molecules were developed separately to enhance drug solubility. The NSs were freeze-dried and the powder form was incorporated directly in an aqueous polymeric blend with poly-vinyl-pyrrolidone for MN-ART and a sodium hyaluronate hydrogel for MN-LUM. The *in vivo* bioavailability studies were performed using a MN reapplication scheme (1 × a day for 3 days), illustrating that an extended-release profile was achieved for both drugs when MNs were applied intradermally, and when compared to conventional oral treatment. The ART-LUM oral treatment was used as a positive control. For antimalarial activity, studies with animals infected with 10^6 *Plasmodium yoelii* 17XNL (12 days) were also conducted using female C57BL/6JUnib mice, demonstrating a 99.5% reduction in parasitemia by day 12 post-infection. By abolishing the infection, MN-ART and MN-LUM may serve as a promising controlled intradermal delivery device for antimalarial drugs to be explored in endemic areas.

1. Introduction

Malaria is the most insidious parasitic disease in the world. In 2019, 229 million cases were reported in 87 countries, with 409,000 associated deaths [1]. The vast majority of cases are concentrated in Africa, with 200 million cases representing 93% of the total reports [2]. The

* Corresponding authors.
E-mail addresses: r.donnelly@qub.ac.uk (R.F. Donnelly), maryann.foglio@fcf.unicamp.br (M.A. Foglio).

https://doi.org/10.1016/j.jconrel.2021.03.036
Received 25 November 2020; Received in revised form 11 March 2021; Accepted 26 March 2021
Available online 29 March 2021

most vulnerable group, accounting for 67% of all malaria deaths worldwide, are children under five years old [2]. Moreover, the most recent World Malaria Report released in 2019 highlighted the impacts of malaria during pregnancy, severely affecting foetus' health and leading to preterm birth and low birth weight in 872,000 children [2].

Malaria is caused by *Plasmodium* parasites transmitted by the female *Anopheles* mosquito [1,3]. One of the main issues associated with malaria is the infection with the specific protozoan *P. falciparum,* which can cause progression to severe illness, often resulting in death if untreated [1,3]. Another important concern is the low adherence to conventional therapy and the lack of health infrastructure in endemic areas, especially in Africa, where the disease is predominantly caused by *P. falciparum* (99.7%) [1,2,4,5], and thus the risk of death is high. For malaria infections caused by *P. falciparum,* the gold standard therapy recommended by the World Health Organization (WHO) is artemisinin-based combination therapy (ACT) [1,3].

ACTs include semi-synthetic artemisinin derivative drugs, such as artemether (ART) (Fig. 1A), which eliminates the *Plasmodium* spp. through free radical formation between the endoperoxide group (C-O-O-C) present in ART with the haem present in haemoglobin [6]. The free radicals formed act against the parasite *via* protein alkylation and oxidation or by inhibition of hemozoin formation, killing the parasites inside the erythrocytes by selective toxicity [6,7]. The selective and fast onset of action of ART is essential to rapidly reduce the parasitemia and associated symptoms and to increase the chance of survival of those infected by *P. falciparum*. To eliminate the residual parasites and to avoid the selection of resistant strains, the combination of ART with aryl amino alcohol drugs, such as lumefantrine (LUM) (Fig. 1B), which has a slower onset of action, is necessary [3].

ART-LUM can act using different mechanisms to inhibit the hemozoin formation, killing the parasites-carrying erythrocytes [3]. The mode of action of LUM is not well established, but its most likely mechanism is through inhibition of hemozoin. The presence of the Cl terminal group on LUM inhibits the formation of β-hematin, and the presence of the tertiary amine group can alter the pH of the digestive vacuole of the parasite (pH 4.8), due to its basic character. This also prevents the formation of β-hematin, the precursor to hemozoin. Inhibition of hemozoin is essential for the parasite's survival within red blood cells and thus, without hemozoin, the parasite cannot survive [8].

ART and LUM are considered safe for children above 5 kg, pregnant women after the first semester, and the elderly due to these specific mechanisms of action, which are responsible for a reduction in their toxicity [4]. However, this fixed combination therapy is available only in oral tablets. Nevertheless, oral therapy in malaria treatment suffers from numerous drawbacks such as: i- vomiting is a symptom from malaria, affecting the oral bioavailability of orally ingested ART-LUM; ii- the low oral absorption of ART (around 30%); iii- poor LUM absorption due to a lack of fat-rich food ingestion (low income populations from endemic areas do not always have access to a meal before each dosage); iv- poor patient compliance and treatment adherence [9–11]. Therefore, the development of more patient-friendly formulations, able to avoid the disadvantages associated with oral administration and enhance treatment adherence, such as MN arrays, is an interesting strategy to be explored.

Dissolving MNs (DMNs) are a minimally invasive intradermal drug delivery platform comprised of micron-sized projections (microneedles, MNs) that protrude outwards from, and perpendicular to, a flat base plate [12–14]. Upon application to the skin, these MNs painlessly penetrate the *stratum corneum*, creating microscopic conduits through which drugs can be delivered to the dermal microcirculation [12,15,16]. DMNs represent an alternative approach to deliver drugs with low oral bioavailability through the skin in a minimally invasive and simplistic manner, allowing for self-administration, thereby improving patient compliance [17,18].

DMNs are prepared with hydrophilic biocompatible polymers that dissolve upon contact with the skin's interstitial fluid releasing the associated drug payload into the viable layers of the skin, eventually being absorbed into the bloodstream *via* the dermal microcirculation [12,19]. DMN application does not cause pain or bleeding, and does not generate sharp waste, thus becoming a convenient option in endemic areas and communities with little access to hospitals, ensuring an effective and safe dosage administration [18–20]. Compared with oral dosage forms, DMNs of ART and LUM avoid the first-pass metabolism, potentially improving drug bioavailability, ensuring an effective dose in cases of vomiting or where oral administration is not viable, therefore expanding the accessibility of treatment for children and elderly patients.

One of the most commonly used formulation approaches for poorly-soluble drugs is the formulation of nanosuspensions (NSs) [21]. NS can be obtained by both the bottom-up and top-down approaches, leading to colloidal dispersions of solid drug nanoparticles [22]. Further solvent removal by spray- or freeze-drying leads to powdered re-dispersible materials [19,23], which can be incorporated into MN-based drug delivery systems to ensure their dermal delivery [12]. Since both ART and LUM are poorly water-soluble drugs, their conversion into solid drug nanoparticles is a necessary step prior to their incorporation into DMNs.

In this work, we report for the first time the development of DMNs for intradermal administration of the antimalarial drugs ART and LUM. The physicochemical characterization of these novel systems is presented. Moreover, we evaluated their pharmacokinetic performance in healthy mice as well as their efficacy in *P. yoelii*-infected mice. The technology described here presents an innovative and effective approach for the delivery of antimalarials with low oral bioavailability, and to treat patients with uncomplicated malaria, primarily in low-resource settings.

2. Materials and methods

ART and LUM with >98% purity were purchased from Tokyo Chemical Industry UK Ltd. (Oxford, UK). Pluronic® F108, F127, F88 (P108, P127 and P88 respectively) were obtained from BASF (Cheadle,

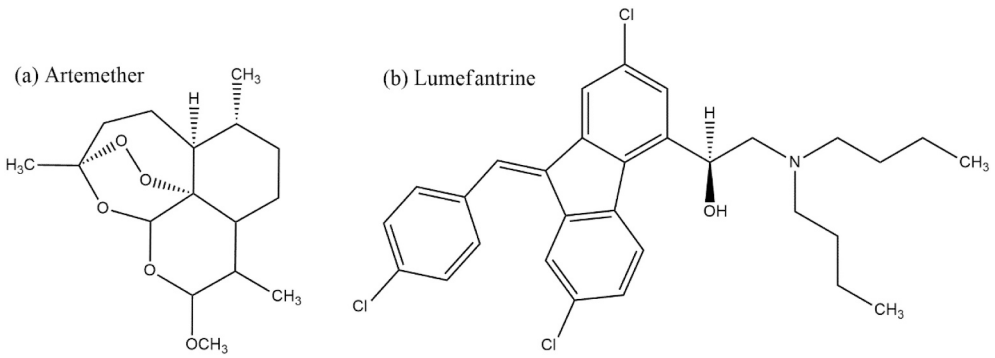

Fig. 1. Chemical structures of (A) artemether and (B) lumefantrine.

UK). Sodium lauryl sulphate (SLS), Polyethylene glycol 180 (PEG) and Polysorbate 80 (Tween® 80, T80), D-(+)-Trehalose dehydrate from *Saccharomyces cerevisiae*, ≥99% (THL), poly(vinyl alcohol) (PVA) mw 13,000-23,000, 98% hydrolysed, trifluoroacetic acid (TFA), poly(caprolactone) mw 80,000 (PCL80) and mw 50,000 (PCL50), and the solvents HPLC-grade solvents chloroform, ethyl acetate, methanol (MeOH) and acetonitrile (ACN), were purchased from Sigma-Aldrich (Gillingham, Dorset, UK). Poly(vinyl pyrrolidone) (PVP), Plasdone™ K-90 and Gantrez™ S-97 (Gantrez) were provided by Ashland™ (Wilmington, DE, USA). Sodium hyaluronate (SHA) Hyabest® (S) LF-P of 99.9% purity, MW 250–400 kDa range was obtained from Kewpie Corporation Fine Chemical Division (Tokyo, Japan). *P. yoelii* 17XNL was obtained from MR4 (catalog number MRA-817, MR4, ATCC Manassas, Virginia, USA). In all cases, Elga purified water was used (Purelab option, Elga LabWater, High Wycombe, UK). All other reagents used in this work were of analytical grade.

2.1. Preparation of ART and LUM nanosuspensions

The nanosuspensions containing ART and LUM were prepared using an optimized anti-solvent precipitation method described previously [24]. Briefly, ART was dissolved in ethyl acetate (120 mg/mL) and LUM in chloroform (120 mg/mL). Using a probe sonicator (Q55, Q Sonica sonicator, Newtown, CT, USA), 5 mL of each organic solution was added drop by drop into 10 mL of an aqueous solution of P108 1%, PEG 6% (for ART), and P108 1%, PEG 8%, SLS 0.5% (for LUM). The sonication parameters were fixed as follows, 80% amplitude was applied for 20 min (for LUM) and 10 min (for ART), with cycles of a 10 s sonication and a 5 s pause. The 20 mL vials containing the aqueous phases were kept in an ice bath during the sonication as illustrated in Fig. 2. Afterwards, both nanosuspensions were magnetically stirred overnight to allow solvent evaporation, leading to a final drug concentration of 60 mg/mL. After particle size determination, the NS was frozen at −80 °C and freeze-dried. The optimization information for both NS is shown in the supplementary data (**Table S1, S2 and S3**).

2.1.1. Freeze-drying

To concentrate both drugs into the DMN tips, the NS were freeze-dried using a Virtis Advantage Bench-top 2.0 freeze-drier system (SP Scientific, Warminster, PA, USA. Prior to introducing the ART and LUM NS to the freeze-drier, 5% (*w*/w) of the cryoprotectants THL or Mannitol were added and dissolved by magnetic stirring. The systems were transferred to suitable vials and freeze-dried for 48 h.

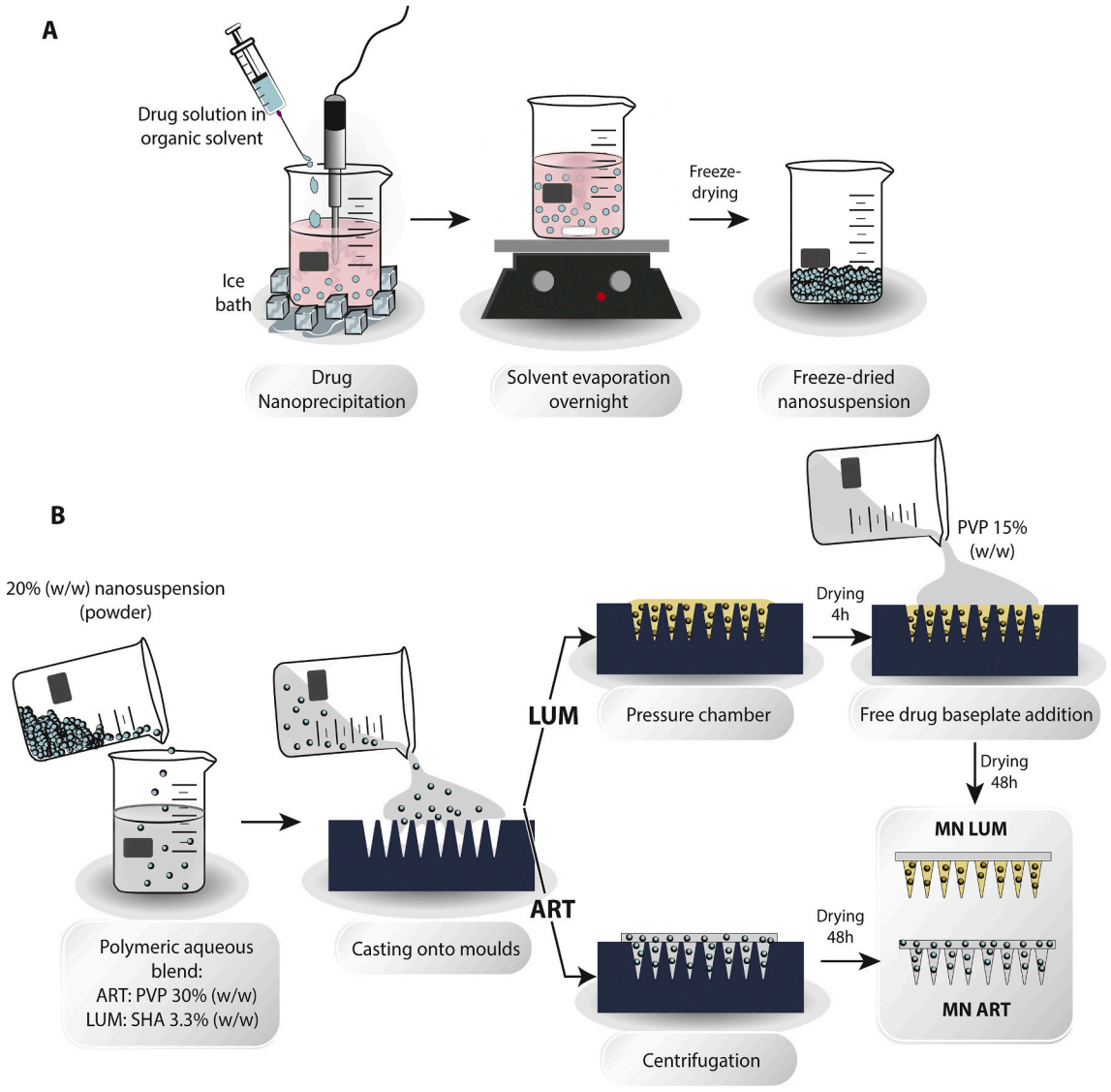

Fig. 2. (A) Schematic representation of nanosuspension (NS) preparation and (B) microneedle (MN) array preparation.

2.1.2. Particle size determinations

Measurements of particle size, polydispersity index (PDI) and zeta potential (ZP) were performed using a Zetasizer Nano ZS (Malvern Instruments, Malvern, UK). The NSs were diluted 10 times using ultra-pure water to obtain the working concentration for analysis. Measurements were carried out at 25 ± 2 °C, at a 90° scattering angle.

2.1.3. Solubility assay

To determine the solubility of the new NSs containing trehalose (NS-T), the respective drugs were initially weighed (10 mg) and dispersed in 1 mL of deionized water and vortexed. Then, more water was added until complete sample dispersion was observed. After complete visual dispersion, the samples were analysed under an optical microscope, filtered and analysed using a HPLC-UV validated method. The experiment was conducted in triplicate.

2.1.4. In vitro release studies

In vitro release studies of ART and LUM NS were carried out using a previously described dialysis methodology [19]. With the aim to ensure sink conditions, different release media was used depending on the solubility of the drugs [25]. For ART, a mixture of phosphate saline buffer (PBS, pH 7.4) and ethanol (1:1) was used, whereas the release media of LUM consisted of 2% T80 in PBS. The study was conducted using the pure drug and the freeze-dried NS (equivalent to 5 mg of each drug). The samples were dispersed in 1 mL of PBS and placed into the Spectra-Por®, 12,000–14,000 MWCO dialysis membrane (Spectrum Medical Industries, Los Angeles, CA, USA). The bags were clamped in both extremes and suspended separately in 50 mL of release media and the systems were then placed at 37 °C at 2 g in an orbital incubator shaker (MaxQ 6000, Thermo Scientific). Samples (1 mL) were withdrawn at predetermined time intervals and replaced with fresh release media. The collected samples were analysed using a validated HPLC-UV method described for each drug (section 2.5 and 2.6), and the amount of drug released were calculated. For all samples, the experiments were carried out using four replicates ($n = 4$).

2.2. Microneedle patches formulation

To optimize the formulation of both ART MNs and LUM MNs (identified as A and L respectively on Supplementary data) a series of blends were prepared separately. The blends were composed of PCL50, and 80, PVP, Gantrez, PVA and SHA polymeric dispersions with either the pure drugs or ART and LUM NS as indicated in **Table S4**. Only the optimized formulations from MN ART and MN LUM are described here, which contained the NS-T formulation for both compounds. It was not possible to prepare MNs containing only the pure drug dispersed in the aqueous hydrogel due to the high hydrophobicity of the drugs, which resulted in a non-homogeneous system.

2.2.1. Artemether microneedles

To prepare MN ART, 500 mg of the resultant aqueous blend containing PVP K-90 30% (*w*/w) and ART NS-T (20% w/w), which consists in the ART-NS freeze-dried with THL (5% w/w), were poured into laser-engineered silicone micromould templates [26] consisting of 361 conical shaped needles (MN density: 19 × 19) with a height of 600 μm, 300 μm width at base and 50 μm interspacing with a total area of 0.49 cm^2. Thereafter, centrifugation at 2054*g* was applied for 15 min to fill the moulds. MN arrays were allowed to dry for 48 h under temperature control (20 °C).

2.2.2. Lumefantrine microneedles

For MN LUM formulations, a two-step method was utilised. To prepare the MNs, the LUM NS freeze-dried with THL (LUM NS-T), was selected as the first formulation layer. The casting process consisted of pouring 100 mg of the chosen aqueous gel containing SHA 3.3% (*w*/w) and LUM NS-T 20% (w/w) onto silicone MN moulds, which were conical in shape and consisted of a 14 × 14 array (600 μm of height, 400 μm width at base and 100 μm of interspacing), with total area of 0.49cm^2 [20]. Then, positive pressure (4 bar) was applied for 30 min. to fill the MN tips containing LUM. Finally, after 4 h of drying the 1st layer, 100 mg of an aqueous blend of PVP (MW 90 kDa) 15% w/w (2nd layer) was poured upon the surface of dried LUM MNs and the positive pressure (4 bar) was applied for 20 min to fill the moulds. MNs were dried for 48 h at 20 °C thereafter.

2.2.3. Optical microscopy analysis

The surface morphology of ART and LUM MNs was evaluated by using optical and digital microscopy. A Leica EZ4D digital/optical microscope and Keyence VHX 700F Digital Microscope (Keyence, Osaka, Japan) were used.

2.2.4. Scanning electron microscopy (SEM)

The morphology of the MNs arrays were evaluated by scanning electron microscopy (SEM) (Zeiss, Evoma-15). MN samples were coated with gold using sputter coater equipment (Bal-Tec, SCDO5O). The morphology of MNs and the mean height of needles were determined (mean ± S.D.) from SEM images using ImageJ® software, where the height of 50 randomly chosen needles from each sample were measured.

2.2.5. Transmission Electron microscopy (TEM)

The morphology and particle size of NS incorporated into the MNs were characterized by TEM according to Colaço et al. [27] using a transmission electron microscope (JEOL, JEM 1400, Tokyo, Japan) [27]. MNs were diluted in deionized water (1:500, MNs: deionized water, *w*/w), and thereafter, the sample was applied to a copper grid (Sigma®, grid size 600 mesh × 42 μm pitch) and dried at room temperature. The measurement of nanoparticles was analysed using ImageJ® software.

2.2.6. Fourier transform infrared spectroscopy (FTIR)

FTIR analyses of the pure ART and LUM, the correspondent NS and MNs were performed using Cary 630 (Agilent, U.S.A) spectrometer, to determine structural changes in the formulation. Attenuated total reflection (ATR) was used with 64 scans for samples and the transmittance was evaluated in wave number from 4000 to 400 cm^{-1}, with 4 cm^{-1} resolution.

2.2.7. Thermal analysis

Differential scanning calorimetry (DSC) was performed using a NETZSCH DSC 200 F3 Maia® (NETZSCH, Geratebäu GmbH, Selb/Germany) differential scanning calorimeter. All procedures were carried out according to methods established previously [5], with a flow rate of 50 mL/min. The sample program progressed from 10 °C to 200 °C at 10 °C/min.

2.2.8. Powder X-ray diffraction

X-ray powder diffraction was carried out to confirm if the ART and LUM within the NS retained their crystallinity. The samples ART, ART NS-T, LUM and LUM NS-T were individually packed into the rotating sample holder and analysed. The experiment was conducted using an X-ray diffractometer (Miniflex™, Rigaku, Neu-Isenburg, Germany) equipped with Ni-filtered, Cu Kβ radiation, at a current of 15 mA and a voltage of 30 kV. The samples were scanned at a range of 3–60° in a continuous mode with a scanning rate of 2°/min.

2.2.9. Mechanical characterization of microneedles

The mechanical strength of DMNs was investigated using a TA.XT2 Texture Analyser (Stable Micro Systems, Haslemere, UK) in compression mode, as previously described [26]. Briefly, MN arrays were attached to a moveable cylindrical probe (length 5 cm, cross-sectional area 1.5 cm^2) of the Texture Analyser and the probe was programmed to move vertically downward at a rate of 1.19 mm/s for 30 s using a 32 N/array force

[28]. The Leica EZ4D digital microscope was utilised for visualization of MN arrays before and after application of the compression test. The heights of individual MNs were measured before and after testing, using the ruler function of the microscope (Leica EZ4 D digital microscope; LAS EZ software; Leica, Wetzlar, Germany). In order to evaluate MN insertion, an established artificial skin-model Parafilm M® was used [28]. Briefly, eight layers of Parafilm M® (Bemis Company Inc., Soignies, Belgium), 126 μm each layer, totalling 1008 μm were used to measure the potential of MNs to penetrate the skin. MNs were inserted into eight-layers of folded Parafilm M® sheets using the Texture Analyser, at a 32 N/array force for 30 s. After the insertion, the MN arrays were removed from the Parafilm M® layers and the number of holes in each layer was evaluated under a digital microscope and two polariser filters.

2.2.10. Dissolution of MNs into the skin studies

The dissolution rate of MNs in the skin was investigated, according to a method described by Permana et al. [19]. The dissolution of the MNs was investigated *in situ* using full thickness skin from stillborn piglets. Skin samples were carefully shaved, fixed to tissue paper with PBS (pH 7.4) at 37 °C and fixed with tacks. After 15 min the MNs were inserted into the centre of the skin using manual pressure. MNs were removed and separated from the skin at different time points (15, 30, 60, 90 and 120 min) and immediately viewed under a Leica EZ4 D microscope.

2.2.11. Drug deposition of MNs into full-thickness skin

Ex-vivo deposition of ART and LUM loaded DMNs, was performed using excised neonatal porcine skin, as previously reported by Donnelly *et al* using $n = 5$ samples per group to determine the amount of drug deposited into the skin layers following 24 h of MN application [19]. For skin deposition studies, full thickness skin was used, and the MNs were applied into the centre of the skin using manual pressure (2.2.10). The MNs were removed after 24 h and the surface of skin was carefully wiped with a damp tissue to remove excess formulation. The samples were then cut to 1 cm^3 and placed into a silicone mold. Thereafter, O.C.T. media (Tissue TEK®) (cryoprotector) was poured into the silicone mold and the skin was frozen with liquid nitrogen. Subsequently, the samples were placed into a microtome to cross section the skin tissue. The cryostatic microtome (Leica CM1900, Leica Microsystems, Nussloch, Germany) environment with stage operated at −25 °C. The samples were positioned so that the upper surface, to which MN patches had been attached, were parallel to the slicing motion of the blade. Slice thickness was set at 50 μm. Five consecutive slices were taken and placed into the same Eppendorf tube (total depth of slicing was approximately 2.5 mm).

For drug quantification, the drug was extracted in 1 mL of organic solvent, which was added into the Eppendorf containing the samples: a) acetonitrile (ART) or b) acetonitrile: acetic acid (100:1) (LUM), followed by sonication for 2 h, centrifuged (10,481 *g*/5 min) and analysed by HPLC using the method detailed in section 2.5–2.6.

2.2.12. Histopathological analysis

Following mice euthanasia, the skin tissue in contact with the MNs was removed using a sharp scalpel blade and transferred to plastic vials with formalin (10% *v*/v). Briefly, the skin samples were sectioned using paraffin-embedding [29] and sectioned at 5 μm using an automated tissue processor (Leica Tissue Processor HistoCore Pearl). The histological staining procedure was performed using the standard protocol for hematoxylin & eosin [29]. The skin samples were examined using a Zeiss Axiophot light microscope (Zeiss, Oberkochen, Germany).

2.3. Pharmacokinetic studies

In vivo drug delivery assessment was undertaken to monitor drug delivery from dissolving MNs containing ART and LUM NS in female 6–7 week old C57BL/6JUnib mice weighing 28.80 ± 2.52 g. The *in vivo* studies were undertaken in compliance with the Ethics and Animal Utilization Committee at UNICAMP under the authorization code 2018/4960–1. Animals were allowed to adapt to the laboratory environment for 7 days prior to study commencement. Prior to the experiment, the backs of the mice were shaved using an animal hair removal cream (Veet®). Four groups were used and MNs were applied in two of the five groups: (1) Reapplication group (1 patch 0.98 cm^2/day/3 days): 1 MN ART (0.49 cm^2) + 1 MN LUM (0.49 cm^2) were applied every 24 h for 3 days. Group (2) consisted of oral Coartem® tablet administration (*via* gavage) (120:20 LUM: ART/mg/tablet) dissolved in water, resulting in a dosage of 24:4 mg/Kg/weight for each mouse, twice a day for 3 days. The time points of blood collection were: 1, 2, 4, 6, 24, 48 and 72 h after the 1st day of treatment. Two groups were used as a control: group (3) with blank MNs applied and (4) with no drug or MN application. For each arm of the study, 7 mice were used.

2.3.1. Drug extraction from plasma matrix

Whole blood was collected from mice into tubes containing 10 μL of EDTA. To separate the plasma, tubes were centrifuged at 1509 *g* for 10 min at 4 °C. To extract ART and LUM from plasma samples, 50 μL of plasma was added into an Eppendorf with 150 μL of ACN acidified with 0.5% (*v*/v) of glacial acetic acid. The samples were vortexed for 60 s and, sequentially, centrifuged at 16,770 *g* for 5 min at 4 °C. The supernatant was collected and analysed by using the HPLC validated method described in 2.5 and 2.6.1.

2.4. Quantification of ART (HPLC-UV)

ART was quantified based upon a previously described and validated method [5,30]. The method described was validated according to the International Conference on Harmonisation (ICH) [31]. Quantification of *in vivo* and *in vitro* ART samples was performed using reverse-phase HPLC-UV. An Agilent 1200® series system (Agilent Technologies UK Ltd., Stockport, UK) was used for all analyses. Agilent ChemStation® Software B.02.01 was used for chromatogram analysis. Chromatographic separation was achieved using an Agilent XDB C_{18} column (50 × 4.6 mm (i.d.) with 1.8 μm packing) with UV detection at 210 nm. The mobile phase consisted of 20:80% (*v*/v) deionized water (acidified with 0.05% (v/v) of trifluoracetic acid): acetonitrile (ACN), pH 2.35. The run time was 6 min in the isocratic mode, the flow rate was 0.6 mL/min and the injection volume was 20 μL. The column temperature was kept at 30 °C. The ART calibration curve was run with ART concentrations in the range 15.125–500 μg/mL, dissolved in HPLC grade ACN.

2.5. In vitro quantification of LUM (HPLC-UV)

LUM was quantified using a validated method developed to analyse *in vitro* samples [30]. Quantification was performed using HPLC-UV (1200® series system (Agilent Technologies UK Ltd., Stockport, UK), with a Polymer X 100 A column (150 × 4 mm (i.d.) with 5 μm), with UV detection at 335 nm. The mobile phase consisted of 30:70% (*v*/v) deionized water (acidified with 0.05% v/v of trifluoracetic acid): ACN in the isocratic mode for 10 min. The flow rate was 1 mL/min, the volume of injection was 20 μL and the column temperature was kept at 30 °C. The LUM calibration curve was prepared in the range of 1.25–100 μg/mL, dissolved in ACN: acetic acid (100:2 v/v).

2.5.1. In vivo quantification of LUM (UPLC-MS)

Quantification of LUM *in vivo* was carried out using a validated method [31] developed in a UPLC system autosampler (Xevo TqD® Waters® Acquity, Waters Corp., Milford, MA, USA), with detection measured by multiple reaction monitoring (MRM) of the mean LUM íon *m/z* 530 and of the daughter ion *m/z* 348. Chromatograms were analysed using MassLynx software. The mobile phase used was A (0.1% formic acid) and B (methanol LC-MS grade), using a gradient system: 0–3 min, 60–100% of B with flow at 0.4 mL/min followed by an increase to methanol 100% over 4 min, held for further 2 min and equilibrated

for 2 min before starting each injection. The run time was 6 min per sample with a flow rate of 0.4 mL/min and an injection volume of 1.0 μl. Mass Spectrometer parameters consisted of desolvation gas flow (N_2) 300 L/hora, desolvation temperature (200 °C), collision gas flow (Ar) 1 L/h, ionization source temperature at 150 °C, capillary voltage (3.5 kV) and cone voltage (45 V), in the positive mode. The LUM calibration curve was run with concentrations in the range 10,000–10 ng/mL, dissolved in HPLC grade ACN acidified with 2% of glacial acetic acid.

2.6. *In vivo antimalarial activity in Plasmodium yoelii-infected mice*

In vivo antimalarial activity of MNs was assessed in groups of 7 female C57BL/6JUnib mice obtained from the Center for Bioterism – UNICAMP (authorization 2018/4960–1 in compliance with the Ethics and Animal Utilization Committee at UNICAMP). Mice were housed in polypropylene cages in a pathogen-free animal care facility 7 days prior to experiments. On day 0, mice were infected *via* intraperitoneal injection with 10^6 GFP-expressing *P. yoelii* 17XNL-infected erythrocytes. After 3 h, treatment began by application of MNs following a modified Peter's 4-day suppressive test [32]. MNs ART and LUM, containing 1580 and 1500 μg of ART and LUM, respectively, were applied once a day for 3 days, using a reapplication model. The untreated group received blank MNs containing PVP and SHA polymers. Parasitemia was measured daily by diluting 1 μL of whole blood obtained from tail vein bleed in 100 μL of PBS followed by flow cytometry analysis using 488 nm laser with 540 nm emission filters (FACSCalibur) (BD Biosciences, San Jose, CA, USA) [33,34]. Antimalarial activity was determined as percentage of parasitemia inhibition relative to the untreated group [35].

2.7. *Statistical analysis*

Statistical analysis was performed using GraphPad Prism 6v® software, and all data is presented as means ± standard deviation (SD) of the mean. For NS drug release and drug deposition of MN in the skin, Mann-Whitney *U* test was performed for comparison with pure drug and film, respectively. For bioavailability studies, the software PKSolver was used to calculate the pharmacokinetic parameters. For *in vivo* data, group parasitemia was compared using a one-way ANOVA and Dunnet's post-test. Data was considered statistically significant when $p < 0.05$.

3. Results and discussion

3.1. *Nanosuspension (NS) development*

To prepare the NS, a range of formulations were tested before reaching the final composition of PEG 180 (1% *w*/w), SLS (0.5% w/w), and Pluronic® F 108 8% (*w*/w) for LUM; and Pluronic® F 108 (1% w/w) with PEG 180 (6% w/w) for ART, as described on **Table S1 – S3**. NS of ART and LUM were produced separately by the anti-solvent precipitation technique [24]. Fig. 3 illustrates the NS in the liquid state (NS), in powder form after the freeze-drying process, and containing mannitol (NS-M), or trehalose (NS-T) at 5% (w/w) as cryoprotectants.

After the freeze-drying process, the particle size, polydispersity index and zeta potential were measured for the NS formulations containing THL or MNT. It was observed that the particle size was higher for the freeze-dried NS containing MNT (ART 364.40 ± 227.20 nm, LUM 1550.08 ± 324.07 nm) when compared with THL (ART 148.10 ± 4.27 nm, LUM 321.00 ± 16.50 nm). Formulations containing THL provided particle size, polydispersity index and zeta potential measurements that were within the preferred range [24] compared to formulations containing MNT.

In addition, after freeze-drying, the dispersion capacity of ART and LUM NS was enhanced when THL was used as a cryoprotectant. Moreover, the present selected NS formulations were able to increase the apparent drug solubility in water of both hydrophobic drugs, allowing drug incorporation into the hydrogel. LUM (pure drug) is poorly soluble in water ($3.09e^{-05}$ mg/mL), and the present LUM NS-T presented an apparent solubility of 0.156 mg/mL in water, and ART NS-T presented an apparent water solubility of 6.52 mg/mL against pure ART (0.457 mg/mL) (Fig. 4C and D). Due to the suitable particle size and dispersion capacity of the NS containing THL as a cryoprotectant, the formulations ART NS-T and LUM NS-T were used in the following studies.

3.1.1. *In vitro drug release studies*

The profiles of *in vitro* release of pure drugs and the NS-T developed are illustrated in Fig. 4A, B and Table 1. The novel ART NS-T indicated less release variation when compared with ART pure drug, due to the NS system, without significant differences after 24 h ($p = 0.0892$). A rapid release profile for ART was observed in the ART NS-T and pure drug groups, with 71% of the total drug released in the first 3 h in the ART NS-T group and 73% of the total drug released in the first 4 h in the ART pure drug group. The burst release observed for both the pure drug and NS formulation can be explained by a discussion of the physicochemical properties attributed to ART [5]. ART is a semisynthetic derivative of artemisinin and is classified as sesquiterpene [36]. Terpenes occur naturally in plants and can act as permeation enhancers, encouraging the diffusion of compounds across biological tissues because of their structural characteristics [37,38]. The terpenes are classified as monoterpenes (C10), containing 2 units of isoprene; sesquiterpenes (C15), which contains 3 units of isoprene, and diterpene (C20), which contains 4 units of isoprene [5,38]. ART is a sesquiterpene containing 2 unsaturated rings and 1 lactonic ring [5]. These types of compounds with an unsaturated ring structure help to enhance skin penetration when compared to a saturated ring structure [5,38].

Regarding the release of samples containing LUM, the LUM NS-T released 5.2 fold more drug, compared with the LUM pure drug. This difference was considered statistically significant (***p value = 0.0002). The release profile of LUM (48 h) was longer than ART (24 h), most likely due to the physicochemical characteristics of LUM, which results in a slower release profile [9,39]. This slow release profile is desirable

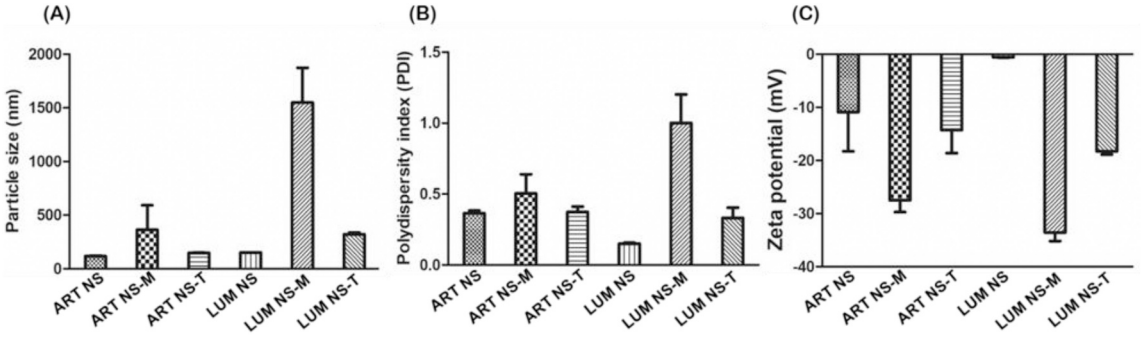

Fig. 3. Comparison of particle size (A), polydispersity index (PDI) (B), and zeta potential (C) from liquid formulations before (ART NS and LUM NS), and after freeze-drying containing the cryoprotectants mannitol (5% w/w) (ART NS-M or LUM NS-M) or trehalose 5% (w/w) (ART NS-T or LUM NS-T).

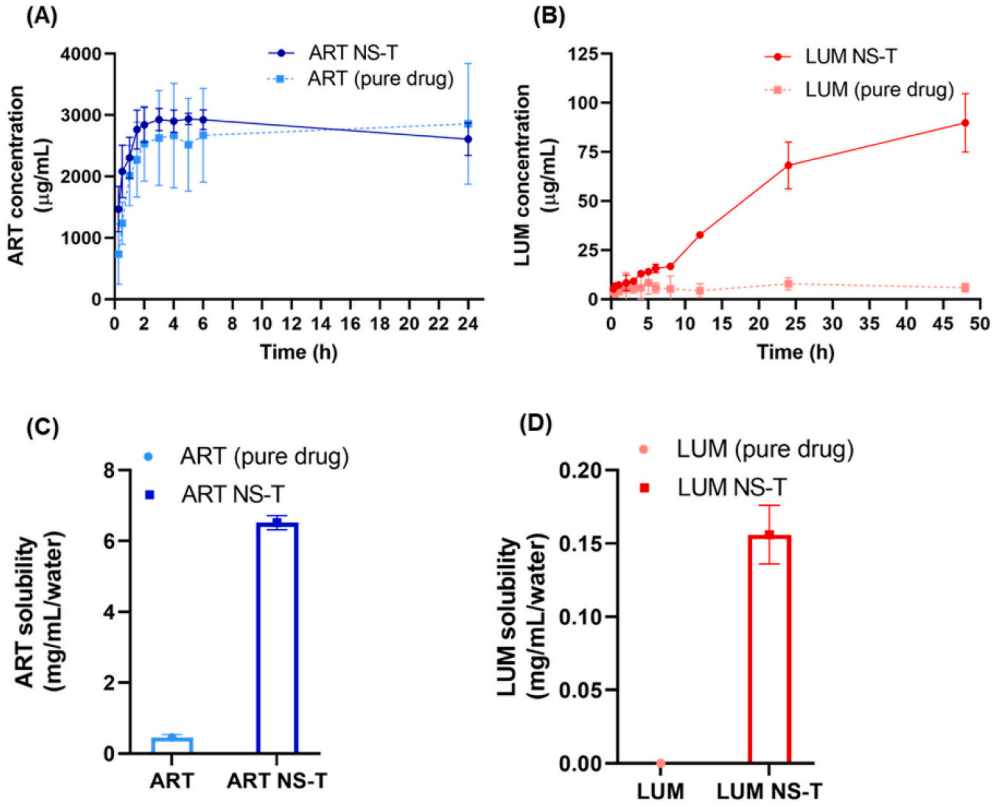

Fig. 4. The concentration of drug release from dialysis membrane studies over 24 h for (A) ART (pure drug) and ART NS-T samples and 48 h for (B) LUM (pure drug) and LUM NS-T, in 50 mL of release media (mean ± SD; $n = 6$). (C) ART (pure drug), ART NS-T and (D) LUM (pure drug) and LUM NS-T saturation solubility in deionized water. Results expressed in mg/mL/water (mean ± SD; $n = 3$).

Table 1
Release profiles of pure drug and drug-containing nanosuspensions from dialysis membranes after 24 h. (means ± SD, $n = 6$).

Sample	Initial amount of drug (μg)	Total μg of drug released after 24 h (μg)	Percentage of drug released after 24 h (%)
ART NS-T	4120.02 ± 129.00	3580.05 ± 156.22	86.93 ± 3.78
ART (pure drug)	3394.09 ± 819.08	2844.24 ± 992.08	81.84 ± 7.90
LUM NS-T	2220.10 ± 12.12	286.98 ± 28.42	12.92 ± 1.30
LUM (pure drug)	2200.02 ± 246.22	54.78 ± 22.02	2.49 ± 1.28

for a partner drug in an ACT formulation, as it targets residual parasites following the potent and fast action of ART and derivatives [9]. The improved release profile for LUM NS-T in comparison with LUM (pure drug) occurred due to the reduced particle size obtained by the NS development process, which increases the effective surface area available, thus enhancing drug dissolution rate according to the Noyes and Whitney Eq. [40]. Additionally, the enhanced release rate of drug exhibited by NS is likely due to the presence of the polymers and surfactants that are able to provide a stabilising effect, particularly F108, which contains PEO-PPO-PEO chains [41]. The hydrophobic chain poly (propylene oxide) (PPO) allows the polymer to adsorb on the surface of hydrophobic drugs, and the hydrophilic chain poly (ethylene oxide) (PEO), extends the steric stabilisation into the aqueous phase by inhibiting NS aggregation [41], improving drug release, dispersion capacity and drug diffusion through the dialysis membrane [40]. Furthermore, PEG 180 can adsorb onto the particle, thereby extending drug release [42]. SLS was used to improve the drug dissolution, preventing LUM self-aggregation and reducing the surface tension, resulting in an increased wettability of the drug particles [43,44].

The release of ART from the NS (87%) was found to be much greater than LUM NS (13%) (**p value = 0.0020). This is due to the different chemical properties of both molecules [45]. ART is a hydrophobic compound, a terpene derivative with a log P of 3.02 and low molecular weight (298 g/mol). The drug is composed of two unsaturated rings and one lactone ring, which helps to facilitate drug release through skin tissue when compared with compounds containing a saturated ring and with a higher molecular weight [46], such as LUM which has a molecular weight of 528 g/mol, a high log P (9.19) and a structure containing 3 saturated rings [5,47]. These unfavourable parameters prevent a satisfactory drug release profile from being achieved. Aqueous solubility must be considered when developing a new drug delivery system as a reasonable level of aqueous solubility is required for transdermal drug delivery to be a success [42], as the drug must diffuse into the "gelled water" of the dermis to be uptaken into the systemic circulation. The formulation of NSs led to an increased dissolution rate, with a sharper effect on LUM. The reduction on the particle size and consequent increase in the specific surface of the drugs, together with the presence of polymers and surfactants produced and enhanced dissolution behaviour, making NSs a viable strategy for the release of these hydrophobic drugs into the viable layers of the skin using MNs.

3.2. Microneedles development

3.2.1. ART microneedles

The selected MN formulation containing ART was composed of an aqueous blend containing PVP K-90 30% (*w*/w) and ART NS-T 20% (w/w). The screening processes used for MN development and prototype formulation development are described in **Table S4** and **Table S5**. The high concentration of PVP K-90 was necessary due to the ART capacity

to form hydrogen binding and also *van der Waals* interactions [48,49], resulting in flexible MNs when a low polymer concentration was used. Other polymers such as Gantrez® S-97, PVA and PCL, were used in the development process, however, only PVP K-90 was able to form mechanically robust MNs, with a view to becoming scalable for manufacturing purposes. Fig. 5 shows (A) digital microscopy analysis, (C) scanning electron microscopy from MN ART formulation prepared from an aqueous blend containing PVP K-90 30% (*w*/w) and ART NS-T 20% (w/w) and (E) MN ART dissolved in water (1: 500 w/w) and submitted to transmission electron microscopy (TEM), allowing visualization of the presence of the NSs. The images show that the NSs remained on the nanoscale (92.6 ± 34.5 nm) after the incorporation of the chosen polymeric matrix.

The DLS analysis confirmed the results, however, there was a slight difference in average particle size 132 ± 69.71 nm, PDI 0.3 ± 0.06, and zeta-potential −14.4 ± 1.65 (Table 2) when compared to TEM. The TEM image information, in most cases, did not corroborate with the data analyses obtained by DLS. DLS and TEM are fundamentally different techniques; in DLS the analysed samples were solvated, in TEM the samples must be diluted and dried, forming a film, to be analysed under ultra-high vacuum conditions [50]. Therefore, DLS provides information on dispersed particles, whereas TEM presents results related to the number of incident electrons that were transmitted through the sample [51].

3.2.2. LUM microneedles

The MN LUM formulation development process is described in **Table S4** and **Table S5**. Polymers such as PCL, PVP, PVA and SHA were used to develop the LUM formulation with a high drug concentration loaded in the tips. However, only SHA was able to form robust MNs with the highest drug concentration (1500 μg) and able to release the higher amount of drug when applied to *ex vivo* porcine skin during the deposition experiment (**Fig. S1**), justifying the need to develop the selected formulation. The final formulation for MN LUM was comprised of an aqueous blend of SHA 3.3% (w/w) with LUM NS-T 20% (w/w).

For MN LUM, bilayer MNs were prepared by using positive pressure. Prior to this, the time taken to form the MN arrays was altered: 5, 10, 15, 20 and 30 min. The time required to obtain fully formed MNs using a viscous gel composed of 3.3% (w/w) SHA 20% (w/w) LUM NS-T was approximately 15–20 min. The second layer, without the drug, composed of PVP K-90 20% (w/w), was applied after the first layer. This two layer casting method was applied for LUM. As this drug has a high molecular weight (528 g/mol) and hydrophobicity [9,52], a reservoir on the top was not required, therefore the methods used herein were able to avoid drug waste and provided robust support to the MNs as a baseplate.

Digital microscopy and scanning electron microscopy (SEM) was used to analyse the morphology of LUM MNs (Fig. 5 **B, D and F**), and transmission electron microscopy (TEM) was used to ensure the nanostructures present in LUM NS-T incorporated into MNs remained on the nanoscale. This was found to be the case, the nanostructures were found to measure 419 ± 25 nm in length by TEM analysis (Fig. 5 **E**), and were found to measure 424 ± 32 nm in length by DLS. Formulating drugs within NSs can improve the bioavailability of lipophilic drugs, reducing the dissolution time and saturated solubility of the drug in the system [35]. In addition, this decreases the dose required to exert therapeutic

Table 2
Particle size, PDI and zeta-potential of various NS formulations in the liquid form, the lyophilized form and loaded into the final MN formulation (means ± SD, $n = 3$).

Formulation	Particle size (nm)	PDI	Zeta-potential
ART NS (liquid ART NS)	118.00 ± 5.09	0.36 ± 0.02	−10.90 ± 7.37
*ART NS-T (freeze-dried ART NS)**	148.10 ± 4.27	0.37 ± 0.04	−14.30 ± 4.30
*MN ART NS-T*loaded = MN ART*	132.00 ± 69.71	0.30 ± 0.06	−14.40 ± 1.65
LUM NS (liquid LUM NS)	151.00 ± 1.76	0.15 ± 0.01	−0.584 ± 0.07
*LUM NS-T (freeze-dried LUM NS)**	321.00 ± 16.50	0.33 ± 0.07	−18.3 ± 0.58
*MN LUM NS-T*loaded = MN LUM*	419.00 ± 25.00	0.33 ± 0.02	−3.45 ± 0.44

* *freeze-dried with 5% (w/w) trehalose.*

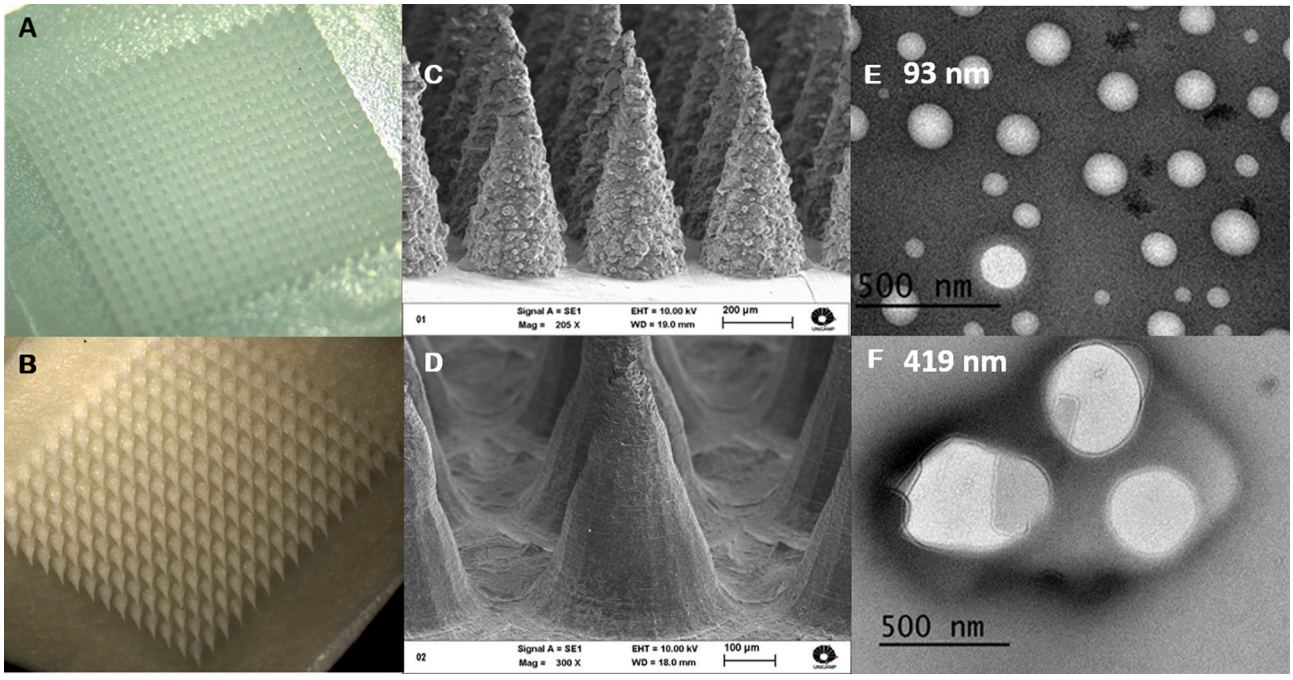

Fig. 5. Digital microscopy images from (A) MNs ART: PVP k-90 30% ART NS-T 20%) and (B) MNs LUM: 3.3% w/w SHA + 20% w/w LUM NS-T (8×). (C) SEM (Scanning Electron Microscopy) images of MNs ART (205×) and (D) MNs LUM (300×); (E) TEM (Transmission Electron Microscopy) images of NSs incorporated into the (E) MNs ART (50,000×) and (F) MNs LUM (50,000×).

effects and, consequently, by reducing the risk of toxicity, this reduces the likelihood of possible side effects [53].

3.2.3. Fourier transform infrared spectroscopy (FTIR)

Infrared analysis is one of the principal techniques used for structural characterization, able to identify the main functional groups in organic compounds present in samples. This is useful for the identification of interactions between drugs and excipients [54]. The ART and LUM spectra (Fig. 6A and B) showed the characteristic organic group for each compound. From the NS spectra of both drugs the characteristic peaks of each drug component indicated some interaction phenomenon between drug and polymers, particularly with ART for ART NS-T, as confirmed by DSC analysis. However, the interaction was not observed for MNs ART as confirmed by DSC analysis and FTIR, indicating that the interaction between the polymer and ART was reduced or inhibited after the incorporation into the PVP polymeric matrix. This interaction phenomenon can be observed, in the spectra of the drugs, formulations and excipients (Fig. 6) and confirmed with DSC (Fig. 7) and XRD (Fig. 8).

The ART spectrum can be seen in Fig. 6A, where at 2800 cm^{-1}, the first stretch referring to C—H (sp^3) occurs, characterized by the generation of bands below 3000 cm^{-1}, overlapping with Pluronic F108 and PEG 180 (Fig. 6C) and MN ART (Fig. 6E). Sequentially, the next band at

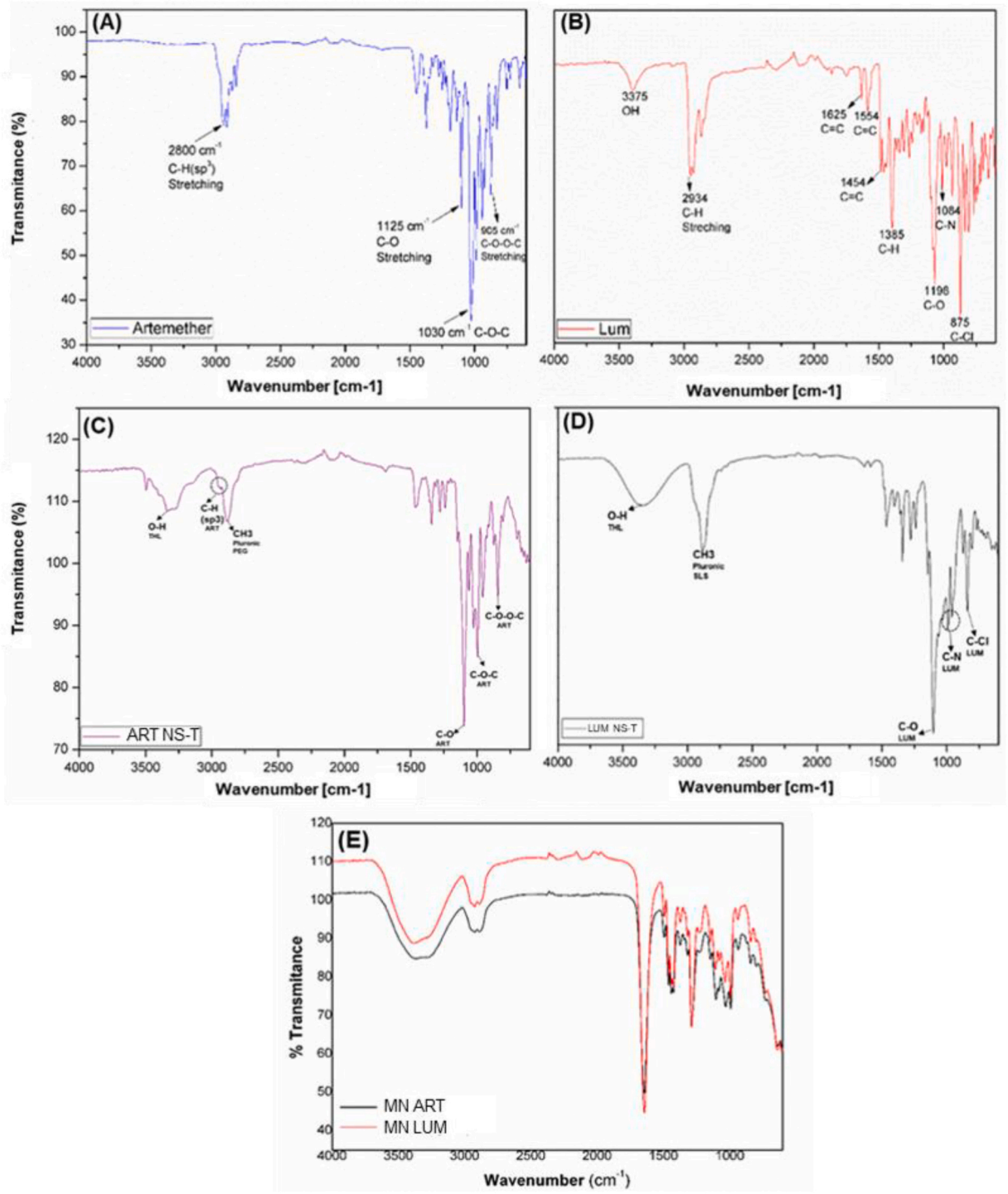

Fig. 6. FTIR spectra of (A) ART, (B) LUM, (C) ART NS-T, (D) LUM NS-T, (E) MN ART and LUM. FTIR obtained in ATR mode.

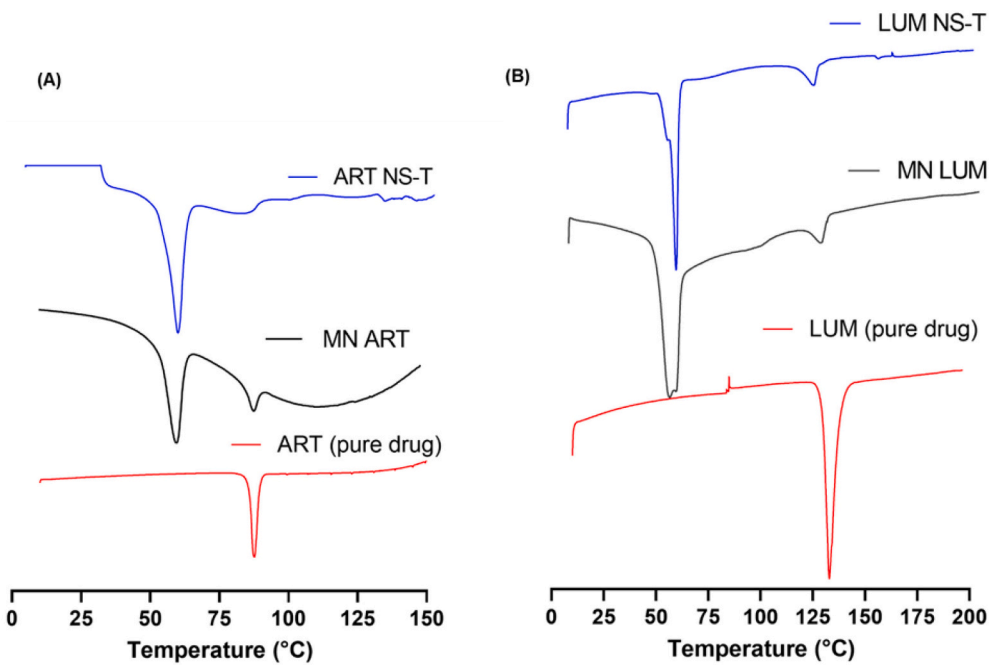

Fig. 7. DSC analysis of (A) ART (pure drug), MN ART and ART NS-T. (B) LUM (pure drug), MN LUM and LUM NS-T.

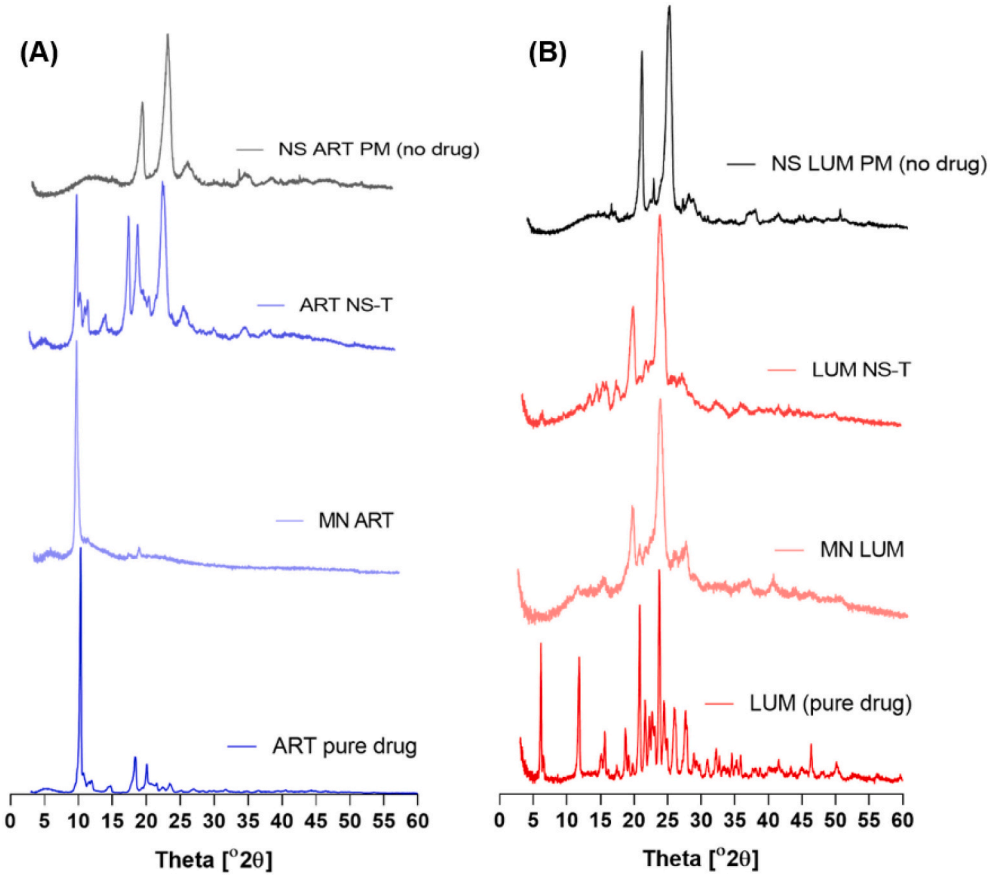

Fig. 8. XRD analysis of (A) ART (pure drug), MN ART, ART NS-T and the physical mix of the excipients present in ART NS-T without drug (NS ART PM (no drug)). (B) LUM (pure drug), MN LUM, LUM NS-T and the physical mix of the excipients present in LUM NS-T with no drug (NS LUM PM (no drug)).

1375 and 1480 cm^{-1}, refers to the stretching of the cyclohexane, and generates symmetrical angular tension (CH) with vibrations referring to the CH_2 of this structure, around 1452 cm^{-1} [55]. The next stretching vibrations from the ART spectrum appear around 1125 cm^{-1} (C—O), referring to a radical bond with –CH-. ART stretching at 1125 cm^{-1} (C—O) refers to a CH-O-CH_3 terminal radical bond. The strong 1030

cm^{-1} band refers to a C-O-C connection present in the ring structure. The band at 905 cm^{-1} refers to the C-O-O-C bonds present in the endoperoxide group [54].

The formation of a band referring to C-O-O-C is fundamental for characterization of artemisinin derivatives, as this is the functional group responsible for the drugs activity. The infrared analyses for this group resulted in a peak below 1200 cm^{-1} and according to experimental calculations described by Moroni et al. [58], the stretching vibration referring to the O—O bonding occurs around 905 cm^{-1}, that is also possible to verify the ring's twisting movement at 943 cm^{-1}. In the present analysis, these peaks were observed at 905 and 959 cm^{-1}, respectively.

Most signals detected between the 1150 and 452 cm^{-1} region can be attributed to C—O bonds, vibrations of the endoperoxide group and other oxygen units present in the ART, which accounts for a total of 5 oxygen units in the structure, and consequently causes a large number of peaks, in addition to different coupling interactions and resonance factors [56,58].

LUM is characterized by the presence of halogen in the structure, due to the bonding of 3 chlorine molecules linked in the top position of the 3 aromatic rings. Besides, there is also the presence of a tertiary amine (Fig. 6B, D and E). The presence of the aromatic ring of LUM is attributed to vibrations present at 1625, 1554, and 1454 cm^{-1}. The experimental spectral data corroborates those reported by Fule et al. [48], presenting the same peaks at 1474 cm^{-1}.

Experimental data described by Fule et al. [48], attributed a peak at 1084 cm^{-1} to the presence of the amine group, in accordance with our data. However, according to Pavia et al. [56] and Silverstein et al. [57] the presence of the amine group can be verified in regions between 1350 and 1000 cm^{-1} (tertiary amine 1345 cm^{-1}), which refers exactly to the fingerprint region of the molecules, which occurs between 1400 and 1000 cm^{-1}. This is unique for each sample and therefore has a greater number of peaks. Therefore, the determination of tertiary amines becomes very difficult by infrared, and other spectroscopic techniques are required [57].

The presence of Cl in LUM occurs between 528 and 698 cm^{-1} [48] and, according to Pavia et al. [56], the presence of chlorine in any substance can occur from 785 to 540 cm^{-1}. The presence of chlorine in the analysis was attributed to a strong vibration peak at 875 cm^{-1} [57].

3.2.4. Thermal analysis

The DSC thermal analysis of ART, MN ART, ART NS-T and LUM, MN LUM, LUM NS-T are represented on **Fig. 7A** and **B**, respectively.

The DSC analysis confirmed that the drugs retained their crystallinity when incorporated into the NS formulation, as confirmed by XRD (Fig. 7). P108 and PEG 180 presented some interference with ART, which is clearly observed in **Fig. S2**. For characterization of the compounds, a comparison was made between the peaks of the pure drug and the peak of the formulations (Fig. 7), and the excipients were compared and confirmed with reported data. Observing the thermogram **(B)**, the first peak is attributed to the presence of PEG 180, clearly visible on **Fig. S3**, with a characteristic melting point at 63.53 °C [59]. Sequentially, the next melting point on the MN ART thermogram refers to the ART melting point, observed at 85.4 °C, which corresponds exactly to the crystalline thermal peak observed in Fig. 7A at 87.7 °C, referring to ART pure drug melting point [60]. The last peak observed on the thermogram **(B)** at 124.8 °C is attributed to LUM, confirmed by DSC of the pure drug at 132.8 °C [61,62].

3.2.5. X-ray diffraction

The crystallinity of drugs and NS systems were studied, as the sonication and lyophilisation process may change the crystallinity of the drug to the amorphous form, and this could interfere directly with drug release and its pharmacological effect once in the body. The diffractograms of the drugs, NS and MN are represented in Fig. 8. In addition, the physical mixture of the NS without drug was investigated to determine any potential interactions which may occur. As reported previously, ART and LUM are crystalline drugs and Fig. 8 confirmed that the crystalline form was retained [47]. Both NS and MN formulations kept their crystalline profile, as is clearly visible on the diffractogram **(A)**, the ART crystalline peak at 10.20° theta for the drug and all the formulations tested. For LUM, the most intense peak at 23.80° theta was present in all the formulations containing LUM **(B)**, confirming that the crystallinity was also retained for both NS and MN formulations.

3.2.6. Insertion and mechanical properties of ART and LUM microneedles

To evaluate the ability of drug containing MNs to penetrate the skin, a simulated insertion study was performed [28]. The percentage of holes created represents the capacity of MNs to penetrate the skin, where each layer corresponds to 126 ± 7 μm thickness [28]. The total penetration depth for MNs LUM and MNs ART was 378 μm (three layers) for both, suggesting that 75.6% of the MN height can penetrate the *stratum corneum* (Fig. 9 **A**).

The results reported in Fig. 9 corroborates with previously reported studies, in which MN insertion was equivalent to 60% of the total MN length [28,63]. The results indicate that these MNs are capable of penetrating the *stratum corneum,* considering the *stratum corneum* thickness is between 10 and 20 μm, excluding the palms and soles of feet which are 400–600 μm in thickness [64]. The next layer of skin is made up of the viable epidermis, which is approximately 100 μm thick [64]. Beyond the epidermis is the dermis, a vascularized layer, where the majority of systemic drug absorption occurs, which is approximately 1200 μm thick [64].

The results from the Parafilm® M study indicate that the MNs were able to penetrate to an approximate depth of 300–375 μm. Therefore the results from this experiment indicated that the MNs were capable of crossing the *stratum corneum* (~ 20 μm) and epidermis (~ 100 μm) Therefore, the results from the study inferred that the drug would be deposited within the dermis, where it would be uptaken by the systemic circulation to exert its systemic effects.

The mechanical characterization was performed by using a compression force of 32 N/array/30s against a metal plate, according to a protocol that simulates finger pressure against the skin with the purpose to guarantee successful skin insertion [28]. According to Larraneta et al. [28], MNs must be strong enough to penetrate the *stratum corneum* and, thereafter, deposit the drug within the skin. Formulation MN ART showed a minimal height reduction of 2.73 ± 1.85% after compression (Fig. 9 (**B**)). For MN LUM, a minimal height reduction of 1.44 ± 0.55% occurred, corresponding with a small decrease when compared to other reported dissolving MNs [17,19], therefore both developed formulations demonstrated that they had adequate mechanical strength for successful insertion into the skin.

3.2.7. Ex-vivo skin dissolution studies

The MN skin dissolution test was undertaken to determine the time required for complete MN dissolution [19].

For MN LUM the total dissolution time was 1 h. The dissolution time of this formulation appeared to be influenced by the physicochemical properties of the drug, which has a high log *P* of 9.19, and is therefore characterized as a highly hydrophobic substance [47], which was synthetised with the purpose to act for a longer duration [11].

For MN ART, the dissolution time was 120 min. The present results corroborate with Qui et al. [65], where MNs containing ART were developed for arthritis treatment using sodium hyaluronate as the chosen polymer, with MNs also dissolving after 120 min. These results indicate that the MNs dissolution time relates to the drug's physicochemical characteristics [65,66].

Considering the rapid action of ART, which reaches the maximum required therapeutic concentration in 2 h after oral dose administration [3,9], the 120 min dissolution time can be considered an appropriate release time for the MN formulations, capable of maintaining ART concentration at a therapeutic level, and of eliminating residual

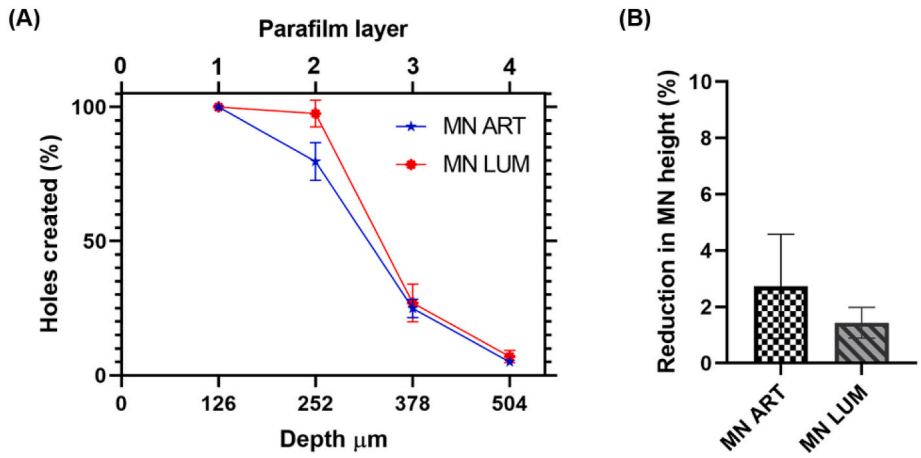

Fig. 9. **(A)** Figure comparing the percentage of holes created in Parafilm® M layers with the approximate insertion depths and number of layers that the ART and LUM MNs were able to penetrate, using an insertion force of 32 N/array (means ± S.D., $n = 5$). **(B)** Percentage MN height reduction, observed following the application of a 32 N/array force (means + S.D., $n = 5$).

Plasmodium together with LUM for a greater duration of action.

3.2.8. *Ex-vivo deposition studies in excised porcine skin*

The deposition of ART and LUM MNs within *ex vivo* porcine skin was investigated. Polymeric films of the same formulation were used as a control. The formulation that achieved the greatest amount of drug release for ART was MN ART, releasing 1197.08 ± 55.07 μg of ART after 24 h, *versus* the film with the same composition, which was able to release only 101.49 ± 17.22 after 24 h. This results in an 11.79 fold increase in ART delivery from the ART MNs when compared with the corresponding film (***p value = 0.0002) (Fig. 10 **A**) (Table 3).

For LUM, drug release into *ex vivo* porcine skin was improved by using LUM MNs, which released 217.05 ± 3.24 μg after 24 h, compared to the drug containing film (without needles), which released 30.19 ± 0.61 μg after the same period. Here, the MN technology was able to improve LUM release by a factor of 7.18 [9,67].

The difference between ART and LUM release may be attributed to the physicochemical differences between both drugs. The large percentage of drug released after 24 h for MN ART (75.80 ± 3.43%) can be explained by ART's ability to permeate intact skin [5,68]. Considering that the total drug content in the MNs matrix was 30,000 μg, with 1580 μg only in the tips, with the highest ART content present in the baseplate, the present results confirm that the drug can diffuse from the baseplate into the skin, because of physicochemical properties of ART [5], as discussed previously in section 3.1.1. The results indicate that penetration into deeper skin layers is possible, as observed in our previous work with ART transdermal bioadhesives [5].

Table 3
Results of *ex vivo* release studies from MN ART and MN LUM after 24 h within excised full-thickness neonatal porcine skin (mean ± SD, $n = 4$).

Samples (formulation % *w*/w)	Drug	drug/ array (μg)	drug/ MNs (μg)	Concentration of drug into the skin (μg)	Total of drug released into the skin (%)
MN ART (PVP K90 30%/ ART NS-T 20%)	ART	30,027 ± 69.5	1580 ± 20.2	1197.08 ± 55.07	75.80 ± 3.43
Film ART (PVP K90 30%/ ART NS-T 20%)	ART	28,447 ± 154	–	101.49 ± 17.22	6.42 ± 0.28
MN LUM (SHA 3.3%/LUM NS-T 20%)	LUM	8806 ± 461	1500 ± 137	217.05 ± 3.24	14.46 ± 0.22
Film LUM (SHA 3.3%/LUM NS-T 20%)	LUM	7306 ± 250	–	30.19 ± 0.61	2.01 ± 0.18

The results from this study illustrate the ability of MN technology to effectively deliver ART and LUM into the skin, and are supported by a previous study [65]. MNs containing ART were previously developed by

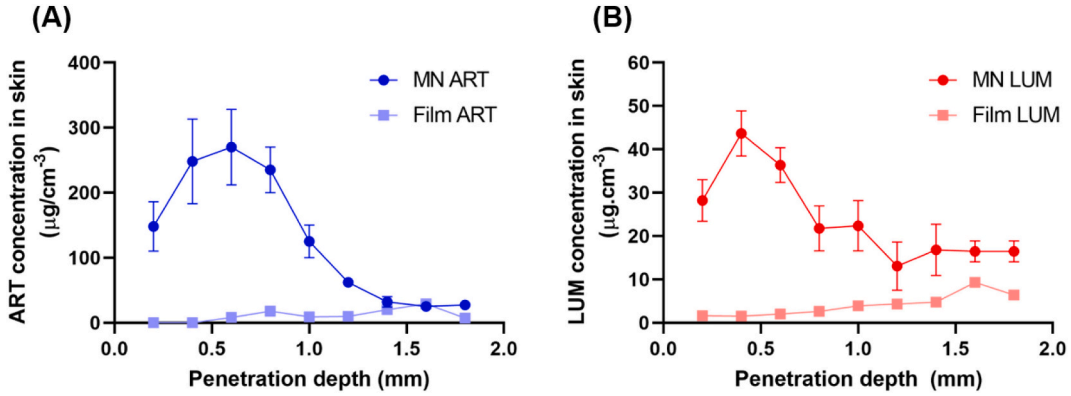

Fig. 10. (A) ART concentration (μg/cm^{-3}) at different penetration depths (mm) within excised full-thickness neonatal porcine skin after 24 h application of either; MN ART, or the drug containing film (without needles, mean ± SD, $n = 4$). (B) LUM concentration (μg/cm^{-3}) at different penetration depths (mm) within excised full-thickness neonatal porcine skin after 24 h application of either; MN LUM, or the drug containing film (without needles, mean ± SD, $n = 4$).

Qiu et al. [65] with 300, 600 and 1200 μg doses for the treatment of arthritis. In animal studies, the authors compared the action of MNs ART with an intramuscular injection (IM) of ART, and found that MN-ART was as effective as the IM injection for the treatment of arthritis, assessed using the arthritic score [65].

3.3. Pharmaceutical analysis

All methodologies used to quantify ART and LUM were validated following ICH guidelines [31]. *In vitro* pharmaceutical analysis was performed using HPLC-UV for both ART and LUM (Table 4). For the *in vivo* analysis, an analytical method with greater sensitivity was required. However, it was only possible to quantify LUM using UPLC-ESI-MS, due the ionization stability of this drug under electrospray (ESI) [69].

For ART samples, it was not possible to use the same methodology, due to stability issues associated with ESI application [70] and as a result, no peak was detected. It was observed that the method failed to detect the intact protonated molecule when ESI was applied [70,71]. In this case, a methodology using atmospheric pressure chemical ionization or tandem MS/MS was required [5,69,70].

3.4. Histological analysis

Histological analysis was performed to evaluate if MNs containing ART and LUM were able to retain skin integrity, or whether the drug containing MNs had the capacity to damage the skin or induce any inflammatory processes. Intact skin was compared with blank MNs (without drug) and with MNs containing ART and LUM for the treatment with MNs 3× (Fig. 11).

Fig. 8**(A)**, **(B)** and **(C)** clearly shows intact skin, without any MN application. In images **(D)**, **(E)** and **(F)**, which correspond to blank MNs, it is possible to see some polymeric material deposited in the skin **(E)** and the MN penetration with polymeric material being expelled from the skin **(F)**. Regarding the skin containing MN ART and MN LUM treatments, the MNs 3× **(G)**, **(H)** and **(I)** presented a long and thin piece of polymer from the MNs, probably due to sufficient MN insertion, as indicated on image **(H)**, and the images **(H)** and **(I)** shows small amounts of residual material deposited in the skin, most likely following polymeric material dissolution in the skin. No inflammatory processes or skin damage was reported in the presented histopathological analysis, indicating that both treatments applied could be considered for further clinical application.

Table 4
Calibration curve properties for LUM and ART detection and quantification *in vitro* and *in vivo* through linear regression and correlation analysis with limits of detection and quantification.

UPLC-ESI-MS (*in vivo*)						
Media	**Drug**	**Slope**	**y-intercept**	**R^2**	***LoD* (ng/mL)**	***LoQ* (ng/mL)**
Plasma	LUM	2.0659 ± 0.12	30,581 ± 0.25	0.9997	7.8	15.6
HPLC-UV (*in vivo*)						
Media	**Drug**	**Slope**	**y-intercept**	**R^2**	***LoD* (μg/mL)**	***LoQ* (μg/mL)**
Plasma	ART	914.14 ± 4.27	7648 ± 8.89	0.998	4.52	11.82
HPLC-UV (*in vitro*)						
Media	**Drug**	**Slope**	**y-intercept**	**R^2**	***LoD* (μg/mL)**	***LoQ* (μg/mL)**
ACN + AA*	LUM	35.254 ± 1.33	−77.658 ± 5.42	0.9998	1.49	4.54
ACN	ART	1.4567 ± 0.02	−2.610 ± 1.02	1	4.10	12.43

* AA = acetic acid 2%.

3.5. Pharmacokinetic performance of ART and LUM MNs

Bioavailability studies were conducted using MN ART and MN LUM formulations, comparing two groups: MN application and oral treatment. For Group 1 (3×), 1 MN ART and 1 MN LUM patch were applied once a day for 3 days, this group is also called the reapplication scheme. The data was compared to the orally treated group (Group 2), in which drug was administered by oral gavage at 4 mg ART / 24 mg LUM per Kg / weight twice a day for 3 days, according to WHO guidelines for curative treatment of uncomplicated *P. falciparum* malaria [72]. The MN formulation was compared with the oral dosage form, the only available treatment option for this drug combination [73].

Fig. 12A and Table 5 shows the kinetics profile of LUM in plasma samples. In the oral administration group, a C_{max} of 2.28 μg/mL after 4 h and C_{min} of 3.09 ng/mL after 72 h was observed (24 mg/LUM/Kg/weight, administered 2×/day for 3 days). In the reapplication group (MN 1×/day/3 days); a C_{max} of 4.34 μg/mL was achieved after 72 h, indicating a cumulative delivery of LUM when daily reapplication of MNs occurred. For MN LUM, the lowest concentration detected was 180 ng/mL after 1 h. When considering that the plasma therapeutic dose of LUM is 200–400 ng/mL [9], the present study demonstrated that therapeutic concentrations of LUM could be delivered *in vivo* using MNs. The use of MNs within this study delivered a higher concentration of LUM than the oral standard fixed combination therapy (ART-LUM 4–24 mg/Kg 2× a day for 3 days).

Comparison of ART MN data with oral therapy was impossible due to the limit of quantification of the analytical methods (HPLC-UV, 7 μg/mL). It is likely that orally administered samples were undetectable using this technique as ART has a low oral bioavailability (20–150 ng/mL) [9,76].

Fig. 12B illustrates the kinetics profile of ART delivered to plasma in rats from MN ART. ART achieved a C_{max} of 431 μg/mL after a 4 h application time and a C_{min} of 92 μg/mL after 24 h, following patch application. When considering that the plasmatic therapeutic level for ART is between 20 and 60 ng/mL [9], this study effectively demonstrated that MN ART was able to deliver a higher therapeutic dosage when compared to oral administration [9,11], and would therefore be effective for the treatment of mice infected with *Plasmodium yoelli*.

Further investigation is necessary for predicting the pharmacokinetics from animal to human. However, based on the body surface area (BSA) normalization method (eq. 1) [74,75], it is possible to extrapolate prudently the information obtained from animal studies and estimate the patch size for human use.

$$HED\left(\frac{mg}{kg}\right) = AD\left(\frac{mg}{kg}\right) x \left(mice\ Km \cdot human\ Km\right) \quad (1)$$

Where, HED (human equivalent dose), AD (animal dose), mice K_m factor (3) and human K_m factor (37).

Considering the plasma therapeutic level of ART, extrapolating between 20 and 150 ng/mL, in line with the concentration of drug delivered within this study, the patch size for ART would be 1 cm^2, containing 3160 μg in the tips and 57,000 μg in the baseplate. This would be enough to deliver an ART dose, which could be considered therapeutic. For LUM, the therapeutic dose for antiplasmodial activity ranges between 200 and 500 ng/mL [9,77]. To achieve the therapeutic plasma level for LUM, a DMN patch containing 35,470 μg in the tips would be required. As this MN, system contains 1500 μg/MN patch and has an array area of 0.49 cm^2, the expected patch size is approximately 12 cm^2.

Consequently, the patch size for a human application containing MN ART (1 cm^2) and MN LUM (12 cm^2) may have approximately 13 cm^2. We expect which the patch will be able to deliver therapeutic amount of drug for both compounds [74,75].

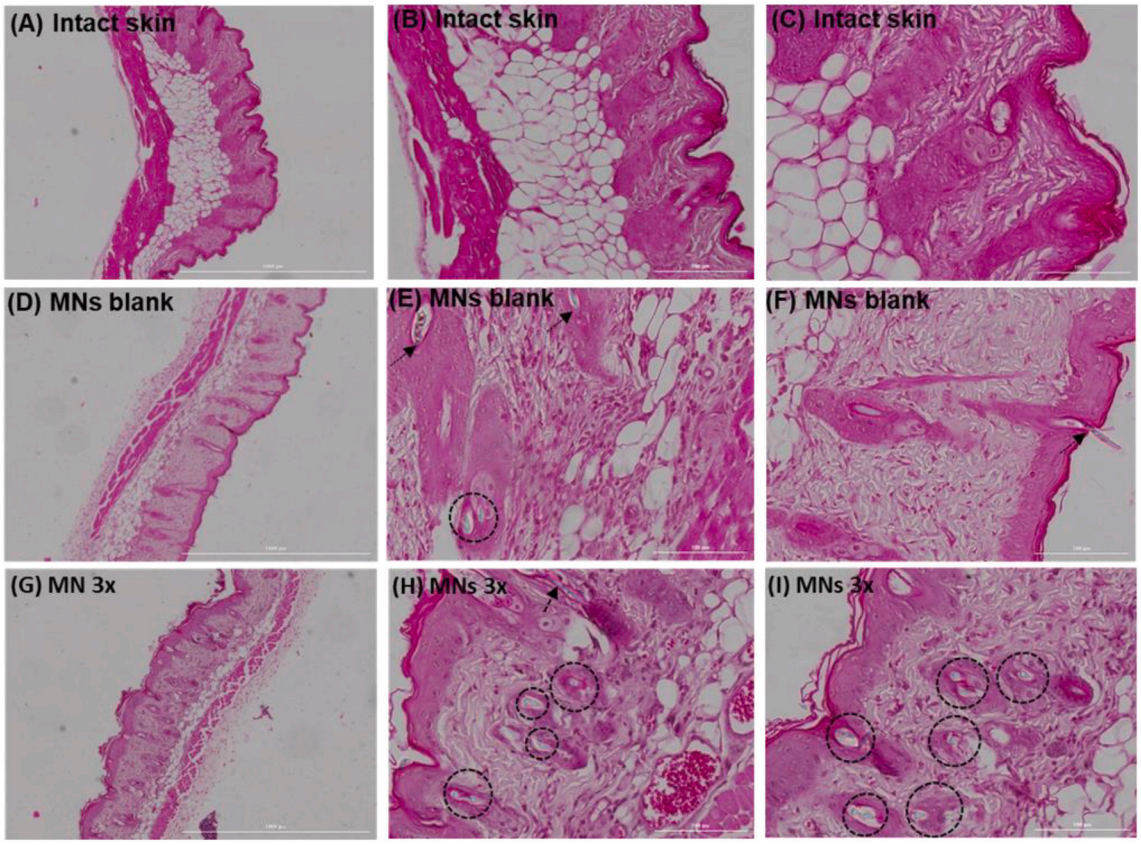

Fig. 11. Histopathological analysis of intact skin (A, B, C), blank MNs (without drug) (D, E, F), and "MNs 3×" refers to the daily reapplication of both patches of MN ART and MN LUM for 3 subsequent days (G, H, I). The indicated images in the figures clearly show the polymeric material deposited into the skin.

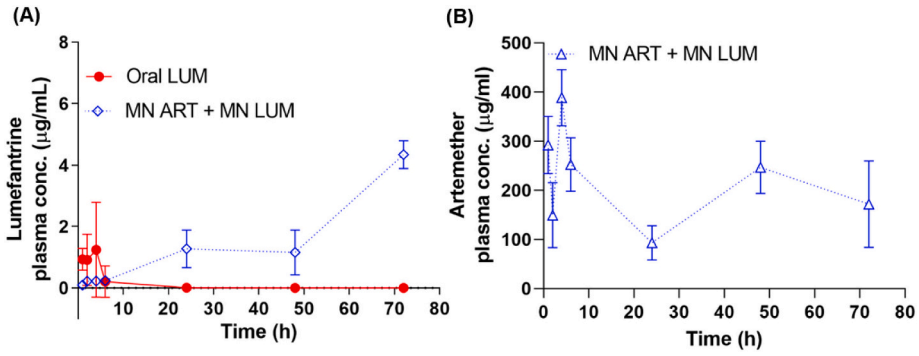

Fig. 12. Pharmacokinetic analysis of (A) LUM and (B) ART, applied to mice as a comparator of WHO recommended oral treatment [72]. The intradermal treatment group was performed using the reapplication scheme dose, applied 1× a day for 3 days (MN 3×). Means ± S.D., $n = 7$. *The oral administration followed the WHO protocol [72] for ART-LUM that includes the oral administration 2 × a day for 3 days with the dosage of 6 mg ART: 24 mg LUM /kg/body weight. The mice dose was defined basis on body surface area, multiplying human dose by the mice factor (0.0026) [45,74,75]. Note: It was not possible to quantify samples obtained from oral treatment for MNs ART, as the analytical methodology applied was not sensitive enough to detect the low concentration of compounds, usually found between 20 and 150 ng/mL/plasma for oral dosage from ART [9].

3.6. *In vivo antimalarial activity in mice infected with Plasmodium yoelii*

After demonstrating the ability of MN ART and MN LUM to cross the *stratum corneum* barrier and reach the bloodstream, we sought to investigate whether the levels of drug in the plasma were within the therapeutic window required for parasite growth inhibition *in vivo*. MNs were applied to *P. yoelii 17XNL*-infected mice in the reapplication scheme 1× a day for 3 days to guarantee the delivery of greater concentrations of LUM and consequently to allow for elimination of residual parasites. The antimalarial activity of ART and LUM is demonstrated in Fig. 13, representative of one experiment conducted.

The application and subsequent reapplication of MNs for three days starting from day 0 was capable of inhibiting, significantly ($p < 0.05$), parasitemia of treated animals when compared to the untreated group (**Table S6**). The graph plotting parasitemia as a function of days post-infection shows that MN application could maintain mice parasitemia below 0.5% throughout the experiment. As shown in Table 6, the MN ART and MN LUM treatment group maintained parasitemia inhibition over 99.5% in all the time points analysed. On day 12, the control group showed 18.8% of parasitemia whereas the group treated with the MNs showed an inhibition percentage of 99.7% - almost fully eliminating mice parasitemia.

The new proposed methodology of patch reapplication once a day for 3 days was vital to improve transdermal LUM delivery, ensuring that the LUM cumulative dosage was enough to eliminate possible remaining parasites. Fig. 10: Comparison of porcentage of microneedles height

Table 5
Pharmacokinetic profiles of MN ART and MN LUM following the reapplication scheme (1 × day/3 days), compared to oral LUM treatment based on the WHO protocol for curative treatment of malaria [72]. Means ± S.D., $n = 7$.

Parameter (unit)	MN ART 3× 1× day/ 3 days	MN LUM 3× 1× day/ 3 days	Oral LUM 2×/day/3 days***
$t_{1/2}$(h)	97.83 ± 68.21	N/A	11.70 ± 3.28
T_{max}(h)	4	72	3
C_{max}(μg/ml)	431.90 ± 68.68	4.31 ± 1.04	2.28 ± 1.02
$AUC_{0\text{-}72}$(μg/ml*h)	14,553 ± 1539	107.86 ± 53.83	7.73 ± 4.65
$AUC_{0\text{-}inf}$(μg/ml*h)	41,080 ± 29,071	N/A	7.80 ± 4.62
MRT (Mean Residence Time) (h)	141.01 ± 103.79	N/A	6.39 ± 2.99

* The oral administration followed the WHO protocol [72] for ART-LUM that includes the oral administration 2 x/day/3 days with the dosage of 6 (ART): 24 (LUM) mg/kg/body weight. The oral mice dose was defined basis on body surface area, multiplying human dose by the mice factor (0.0026) [45,74,75].

** Note: It was not possible to quantify samples obtained from oral treatment for MN ART, due to the analytical methodology applied was not sensitive to detect the low concentration of compounds, usually found for oral dosage from ART between 20 and 150 ng/mL [69].

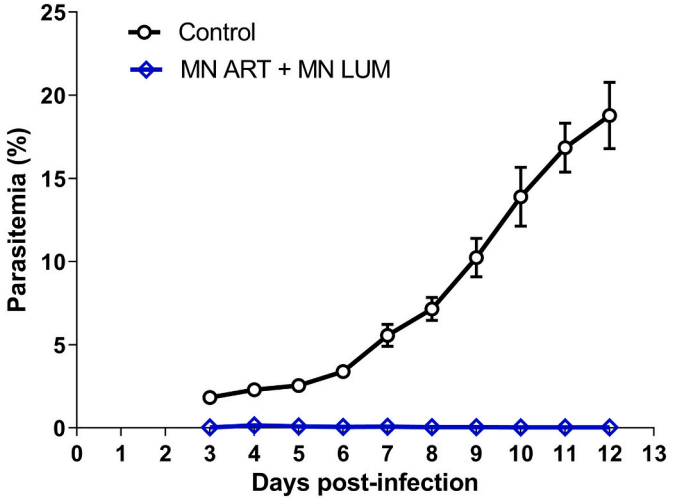

Fig. 13. Peripheral blood parasitemia curves as a function of time to day 12 post-infection in groups of mice infected with murine parasite *P. yoelii* 17XNL. Control group: MN Blank without drug. Treated group: MN ART + MN LUM applied using the reapplication scheme of 1× a day for 3 days. (Mean ± S.D., $n = 7$).

Table 6
Percentage of parasitemia and parasitemia inhibition[a] of mice infected with *P. yoelii* 17XNL treated with MN ART and MN LUM. (Mean ± S.D., $n = 7$). [a]Values are expressed as the mean of parasitemia inhibition in relation to the control.

Parasitemia (Mean ± S.D., %)				
Days post-infection	**D3**	**D6**	**D9**	**D12**
Control	1.8 ± 0.6	3.4 ± 0.8	10.3 ± 2.6	18.8 ± 4.5
MN ART+ MN LUM	0.03 ± 0.02	0.07 ± 0.12	0.5 ± 0.06	0.04 ± 0.04
Parasitemia inhibition (Mean ± S.D., %)				
Days post-infection	**D3**	**D6**	**D9**	**D12**
MN ART+ MN LUM	98.1 ± 1.2	97.9 ± 3.5	99.5 ± 0.6	99.7 ± 0.2

reduction of dissolving microneedles formulations tested, after application of a force of 32 N/array (mean ± SD; $n = 5$). (**A**) Before compression; (**B**) After compression.

According to van Vugt et al. [78], in human studies where ART-LUM tablets (20/120 mg) were given orally, 75% of patients with a LUM plasma concentration above 280 ng/mL on day 7 were cured, compared with 51% of patients with lower plasma concentration of LUM. However, a study by White et al. [9] emphasised the importance of a 7 day treatment duration to cure malaria, as this is essential to achieve a therapeutic LUM plasma concentration of around 500 ng/mL. Studies conducted by WWARN (2015) [77], on the other hand, indicate that a plasma concentration of LUM of 200 ng/ml on day 7 would be sufficient to achieve a 95% cure rate in all patients, including children.

Therefore, the results obtained herein using infected mice, which achieved a C_{max} of ~4 μg/LUM/mL/plasma at 72 h, demonstrated the ability of the novel MN ART and MN LUM regimen to eliminate malaria parasites, when applying only 1 patch/day for 3 days. Therefore, the present results from *in vivo* studies were able to confirm the capacity of MN ART and LUM to release the drug incorporated into the needles through the skin layers into the blood, confirming that the novel formulation was able to effectively eliminate malaria parasites.

Using the MN patch improved the ART bioavailability, extending the release of a drug with a short half-life [9,79]. The present results are promising, especially considering the impact of this new technology application. It is well known that the short half-life is a disadvantage of artemisinin derivatives, requiring the association with a long half-life drug to eliminate residual parasites and avoid the plasmodium resistance [80]. The extended release observed may overcome the plasmodium resistance, characterizing a promising option for malaria treatment. MN technology will be able to reduce the dosage administrated, avoid the first-pass metabolism and improve the drug bioavailability.

Regarding the microneedles cost manufacturing, it is well known that malaria and poverty are closely associated, because the burden of malaria prevents economic growth, increasing inequality and poverty [81]. Actions for malaria prevention reduce mortality, morbidity, and health-care service costs. This allows for more investment in education, food, and quality of life, thus bringing a series of benefits for economic development [81].

The MN patch could reduce the frequency and the number of doses, therefore lowering the price of the treatment. In addition, the technology cost is not a barrier for manufacturing the product. The investment is a potential lifesaver, especially for children under five, who account for 67% of the total deaths [9]. Microneedles technology is a self-administered, painless and safe treatment option for patients in low-resource settings, where access to hospital facilities is extremely difficult. Children have higher acceptability on MNs application when compared with oral or parenteral administration [10–12]. This may increase therapy adherence for the population most affected by malaria, which could reduce the mortality rate. Malaria prevention is an overwhelming challenge; however, it is also a cost-effective business investment.

4. Conclusion

In this work, we reported for the first time the use of DMNs loaded with ART and LUM for malaria treatment and prophylaxis. Both MNs were developed with robust mechanical strength, able to penetrate the *stratum corneum*, and were able to release the drug into the skin for transdermal delivery. The NSs containing ART and LUM were able to improve the solubility of these hydrophobic drugs. The *in vivo* delivery demonstrated that an extended release profile was achievable for both ART and LUM when compared with the oral administration, observing a prolonged duration of action for both drugs using the novel MN design. The animal infection study with *P. yoelii* indicated that the treatment regimen which used MNs ART-LUM strongly inhibited mice parasitemia,

resulting in infection elimination. MNs are a promising technology, which improves the delivery of hydrophobic drugs transdermally in a minimally invasive way, allowing for self-administration of drugs. The novel MNs containing ART-LUM was shown to improve the bioavailability of ART-LUM *via* delivery into the skin, providing a therapeutic dosage for mice infected with *P. yoelii*, reducing the parasitemia level, which is crucial in the first 24 h after symptoms begin if treatment is to be successful. When compared to oral administration, this new drug delivery system could improve the adherence to this therapy; help to reduce the number of fatal cases and improve the access to antimalarials to treat patients with uncomplicated malaria, particularly in remote places with fewer resources and a lack of medical facilities.

Declaration of Competing Interest

The authors have no conflict of interest in this work.

Acknowledgements

The authors would like to thank the Fundação de Amparo à Pesquisa do Estado de São Paulo (FAPESP) grants 2014/16008-3, 2016/18384-8, 2017/18611-7 and 2019/02171-3, and the Conselho Nacional de Desenvolvimento Científico e Tecnolóogico (CNPq) grant 01904/2012-1 for funding, and Capes. MAF & FTMC are CNPq research fellow.

Appendix A. Supplementary data

Supplementary data to this article can be found online at https://doi.org/10.1016/j.jconrel.2021.03.036.

References

[1] W. World Health Organization, World malaria report 2020: 20 years of global progress and challenges., Geneva, 2020 https://doi.org/Licence: CC BY-NC-SA 3.0 IGO.
[2] World Health Organization, World Malaria Report, World Heal. Organ, 2019, p. 238. WHO/HTM/GM. https://doi.org/ISBN 978 92 4 1564403.
[3] T.N.C. Wells, R.H. Van Huijsduijnen, W.C. Van Voorhis, Malaria medicines: a glass half full? Nat. Rev. Drug Discov. 14 (2015) 424–442, https://doi.org/10.1038/nrd4573.
[4] J.D. Challenger, K. Bruxvoort, A.C. Ghani, L.C. Okell, Assessing the impact of imperfect adherence to artemether-lumefantrine on malaria treatment outcomes using within-host modelling, Nat. Commun. 8 (2017), https://doi.org/10.1038/s41467-017-01352-3.
[5] F.V. Zanutto, E. Mcalister, M. Marucci, P. Tangerina, B. Fonseca-Santos, H.C. Salles, M.O. Souza, A. Brisibe, W. Vilegas, M. Chorilli, M. Akira D' Avila, R.F. Donnelly, M. A. Foglio, Semisynthetic derivative of Artemisia annua-loaded transdermal bioadhesive for the treatment of uncomplicated malaria caused by *Plasmodium falciparum* in children, J. Pharm. Sci. 108 (2019) 1177–1188, https://doi.org/10.1016/j.xphs.2018.10.007.
[6] J. Wang, C.J. Zhang, W.N. Chia, C.C.Y. Loh, Z. Li, Y.M. Lee, Y. He, L.X. Yuan, T. K. Lim, M. Liu, C.X. Liew, Y.Q. Lee, J. Zhang, N. Lu, C.T. Lim, Z.C. Hua, B. Liu, H. M. Shen, K.S.W. Tan, Q. Lin, Haem-activated promiscuous targeting of artemisinin in Plasmodium falciparum, Nat. Commun. 6 (2015) 1–11, https://doi.org/10.1038/ncomms10111.
[7] D.A. Estman, R.T. Fidock, Artemisinin-based combination therapies: a vital tool in efforts to eliminate malaria, Nat. Rev. Microbiol. 7 (2009) 864–874.
[8] D.J. Sullivan, Theories on malarial pigment form ation and quinoline action, Int. J. Parasitol. 32 (2002) 1645–1653.
[9] N.J. White, M. Van Vugt, F. Ezzet, Clinical pharmacokinetics and pharmacodynamics of artemether-lumefantrine, Clin. Pharmacokinet. 37 (1999) 105–125, 0312-5963/99/0008-0105/$10.50/0.
[10] K. Banek, M. Lalani, S.G. Staedke, D. Chandramohan, Adherence to artemisinin-based combination therapy for the treatment of malaria: a systematic review of the evidence, Malar. J. 13 (2014), https://doi.org/10.1186/1475-2875-13-7.
[11] F. Kloprogge, R. McGready, W. Hanpithakpong, D. Blessborn, N.P.J. Day, N. J. White, F. Nosten, J. Tarning, Lumefantrine and desbutyl-lumefantrine population pharmacokinetic-pharmacodynamic relationships in pregnant women with uncomplicated plasmodium falciparum malaria on the Thailand-Myanmar border, Antimicrob. Agents Chemother. 59 (2015) 6375–6384, https://doi.org/10.1128/aac.00267-15.
[12] A.J. Paredes, P.E. McKenna, I.K. Ramöller, Y.A. Naser, F. Volpe-Zanutto, M. Li, M. T.A. Abbate, L. Zhao, C. Zhang, J.M. Abu-Ershaid, X. Dai, R.F. Donnelly, Microarray patches: poking a hole in the challenges faced when delivering poorly soluble drugs, Adv. Funct. Mater. 2005792 (2020) 1–27, https://doi.org/10.1002/adfm.202005792.
[13] A.S. Cordeiro, I.A. Tekko, M.H. Jomaa, L. Vora, E. McAlister, F. Volpe-Zanutto, M. Nethery, P.T. Baine, N. Mitchell, D.W. McNeill, R.F. Donnelly, Two-photon polymerisation 3D printing of microneedle array templates with versatile designs: application in the development of polymeric drug delivery systems, Pharm. Res. 37 (2020) 174, https://doi.org/10.1007/s11095-020-02887-9.
[14] P.M. Rezvan Jamaledin, Cynthia K.Y. Yiu, Ehsan N. Zare, Li-Na Niu, Raffaele Vecchione, Guojun Chen, Zhen Gu, Franklin R. Tay, Advances in antimicrobial microneedle patches for combating infections, Adv. Mater. 32 (2020) 2002129, https://doi.org/10.1002/adma.202002129.
[15] R. Jamaledin, C. Di Natale, V. Onesto, Z. Taraghdari, E. Zare, P. Makvandi, R. Vecchione, P. Netti, Progress in microneedle-mediated protein delivery, J. Clin. Med. 9 (2020) 542, https://doi.org/10.3390/jcm9020542.
[16] P.A.N. Rezvan Jamaledin, Pooyan Makvandi, Cynthia K.Y. Yiu, Tarun Agarwal, Raffaele Vecchione, Wujin Sun, Tapas Kumar Maiti, Franklin R. Tay, Engineered microneedle patches for controlled release of active compounds: recent advances in release profile tuning, Adv. Ther. 3 (2020) 2000171, https://doi.org/10.1002/adtp.202000171.
[17] A.D. Permana, Q.K. Anjani, E. Utomo Sartini, F. Volpe-Zanutto, A.J. Paredes, Y. M. Evary, S.A. Mardikasari, M.R. Pratama, I.N. Tuany, R.F. Donnelly, Selective delivery of silver nanoparticles for improved treatment of biofilm skin infection using bacteria-responsive microparticles loaded into dissolving microneedles, Mater. Sci. Eng. C 120 (2021) 111786, https://doi.org/10.1016/j.msec.2020.111786.
[18] L.K. Vora, K. Moffatt, I.A. Tekko, A.J. Paredes, F. Volpe-Zanutto, D. Mishra, K. Peng, R. Raj Singh Thakur, R.F. Donnelly, Microneedle array systems for long-acting drug delivery, Eur. J. Pharm. Biopharm. 159 (2021) 44–76, https://doi.org/10.1016/j.ejpb.2020.12.006.
[19] A.D. Permana, A.J. Paredes, F. Volpe-Zanutto, Q.K. Anjani, E. Utomo, R. F. Donnelly, Dissolving microneedle-mediated dermal delivery of itraconazole nanocrystals for improved treatment of cutaneous candidiasis, Eur. J. Pharm. Biopharm. 154 (2020) 50–61, https://doi.org/10.1016/j.ejpb.2020.06.025.
[20] M.T.C. McCrudden, E. Larrañeta, A. Clark, C. Jarrahian, A. Rein-weston, S. Lachaudurand, N. Niemeijer, P. Williams, C. Haeck, H.O. Mccarthy, D. Zehrung, R. F. Donnelly, Design , formulation and evaluation of novel dissolving microarray patches containing a long-acting rilpivirine nanosuspension, J. Control. Release 292 (2018) 119–129, https://doi.org/10.1016/j.jconrel.2018.11.002.
[21] A.D. Permana, Q.K. Anjani, E. Utomo Sartini, F. Volpe-Zanutto, A.J. Paredes, Y. M. Evary, S.A. Mardikasari, M.R. Pratama, I.N. Tuany, R.F. Donnelly, Selective delivery of silver nanoparticles for improved treatment of biofilm skin infection using bacteria-responsive microparticles loaded into dissolving microneedles, Mater. Sci. Eng. C 120 (2021) 111786, https://doi.org/10.1016/j.msec.2020.111786.
[22] E. Merisko-Liversidge, G.G. Liversidge, Nanosizing for oral and parenteral drug delivery: a perspective on formulating poorly-water soluble compounds using wet media milling technology, Adv. Drug Deliv. Rev. 63 (2011) 427–440, https://doi.org/10.1016/j.addr.2010.12.007.
[23] A. Touzet, F. Pfefferlé, P. van der Wel, A. Lamprecht, Y. Pellequer, Active freeze drying for production of nanocrystal-based powder: a pilot study, Int. J. Pharm. 536 (2018) 222–230, https://doi.org/10.1016/j.ijpharm.2017.11.050.
[24] A.D. Permana, M.T.C. McCrudden, R.F. Donnelly, Enhanced intradermal delivery of nanosuspensions of antifilariasis drugs using dissolving microneedles: a proof of concept study, Pharmaceutics 11 (2019), https://doi.org/10.3390/pharmaceutics11070346.
[25] OECD, OECD Guidance Notes on Dermal Absorption, 2005.
[26] R.F. Donnelly, R. Majithiya, T.R.R. Singh, D.I.J. Morrow, M.J. Garland, Y.K. Demir, K. Migalska, E. Ryan, D. Gillen, C.J. Scott, A.D. Woolfson, Design, optimization and characterisation of polymeric microneedle arrays prepared by a novel laser-based micromoulding technique, Pharm. Res. 28 (2011) 41–57, https://doi.org/10.1007/s11095-010-0169-8.
[27] R. Colaco, M. Clara Goncalves, L.M. Fortes, L.M.D. Goncalves, A.J. Almeida, B. F. Martins, Preparation and chemical characterization of eco-friendly ORMOSIL nanoparticles of potential application in DNA gene therapy, Curr. Nanosci. 9 (2013) 168–172, https://doi.org/10.2174/1573413711309010028.
[28] E. Larrañeta, J. Moore, E.M. Vicente-Pérez, P. González-Vázquez, R. Lutton, A. D. Woolfson, R.F. Donnelly, A proposed model membrane and test method for microneedle insertion studies, Int. J. Pharm. 472 (2014) 65–73, https://doi.org/10.1016/j.ijpharm.2014.05.042.
[29] John Kuo, Electron Microscopy Methods and Protocols, 3rd ed., Humana Press, Totowa, NJ, 2014 https://doi.org/10.1007/978-1-62703-776-1.
[30] I.C. da César, F.H. Andrade Nogueira, G. Antônio Pianetti, Simultaneous determination of artemether and lumefantrine in fixed dose combination tablets by HPLC with UV detection, J. Pharm. Biomed. Anal. 48 (2008) 951–954, https://doi.org/10.1016/j.jpba.2008.05.022.
[31] D.E. Phillip Borman, Q2(R1) Validation of analytical procedures: text and methodology, in: A. Teasdale, D. Elder, R.W. Nims (Eds.), ICH Qual. Guidel. An Implement. Guid, 1st ed., Wiley, Hoboken, New Jersey, U.S.A, 2017, pp. 127–166.
[32] D.A. Baker, L.B. Stewart, J.M. Large, P.W. Bowyer, K.H. Ansell, M.B. Jiménez-Díaz, M. El Bakkouri, K. Birchall, K.J. Dechering, N.S. Bouloc, P.J. Coombs, D. Whalley, D.J. Harding, E. Smiljanic-Hurley, M.C. Wheldon, E.M. Walker, J.T. Dessens, M. J. Lafuente, L.M. Sanz, F.J. Gamo, S.B. Ferrer, R. Hui, T. Bousema, I. Angulo-Barturén, A.T. Merritt, S.L. Croft, W.E. Gutteridge, C.A. Kettleborough, S. A. Osborne, A potent series targeting the malarial cGMP-dependent protein kinase clears infection and blocks transmission, Nat. Commun. 8 (2017) 1–9, https://doi.org/10.1038/s41467-017-00572-x.
[33] T. Ono, T. Tadakuma, A. Rodriguez, Plasmodium yoelii yoelii 17XNL constitutively expressing GFP throughout the life cycle, Exp. Parasitol. 115 (2007) 310–313.

[34] M.T.D. Gabriel, W. Rangel, Martha A. Clark, Usheer Kanjee, Caeul Lim, Kathryn Shaw-Saliba, Maria José Menezes, Anjali Mascarenhas, Laura Chery, Edwin Gomes, Pradipsinh K. Rathod, Marcelo U. Ferreira, Enhanced ex vivo *Plasmodium vivax* intraerythrocytic enrichment and maturation for rapid and sensitive parasite growth assays, Antimicrob. Agents Chemother. 62 (2018) 1–9, https://doi.org/10.1128/AAC.02519-17.

[35] L.T. Ferreira, J. Rodrigues, G. Capatti Cassiano, K.C. do Peralis Tomaz, D.C. Baia-da-Silva, M. Ferreira Souza, M. Mottin, L. Dias Almeida, J. Calit, M.C. Silva de Barros Puça, D. Youssef Bargieri, S. Costa Pinto Lopes, M. Vinicius Guimarães Lacerda, P. Sunnerhagen, B. Junior Neves, C. Horta Andrade, F.T. M. Costa, Computational chemogenomics drug repositioning strategy enables the discovery of epirubicin as a new repurposed hit, Antimicrob. Agents Chemother. 64 (2020) 1–16, https://doi.org/10.1128/AAC.02041-19.

[36] Y. Tu, The discovery of artemisinin (qinghaosu) and gifts from Chinese medicine, Nat. Med. 17 (2011) 1217–1220, https://doi.org/10.1038/nm.2471.

[37] W.R. Kadhum, H. Todo, K. Sugibayashi, Percutaneous Penetration Enhancers Chemical Methods in Penetration Enhancement, 2015, pp. 243–253, https://doi.org/10.1007/978-3-662-45013-0.

[38] N. Kanikkannan, K. Kandimalla, S. Lamba, M. Singh, Structure-activity relationship of chemical penetration Enhan-cers in transdermal drug delivery, Curr. Med. Chem. 7 (2012) 593–608, https://doi.org/10.2174/0929867003374840.

[39] G. Huang, J. Liu, L. Tian, S. Chen, Novel nanostructured lipid carrier for oral delivery of a poorly soluble antimalarial agent lumefantrine: characterization and pharmacokinetics evaluation, MOJ Bioequivalence Bioavailab 5 (2018) 33–38, https://doi.org/10.15406/mojbb.2018.05.00079.

[40] Y. Hattori, Y. Haruna, M. Otsuka, Colloids and surfaces B: biointerfaces dissolution process analysis using model-free Noyes – Whitney integral equation, Colloids Surf. B: Biointerfaces 102 (2013) 227–231, https://doi.org/10.1016/j.colsurfb.2012.08.017.

[41] A. Pitto-Barry, N.P.E. Barry, Pluronic® block-copolymers in medicine: from chemical and biological versatility to rationalisation and clinical advances, Polym. Chem. 5 (2014) 3291–3297, https://doi.org/10.1039/c4py00039k.

[42] B.E. Rabinow, Nanosuspensions in drug delivery, Nat. Rev. Drug Discov. 3 (2004) 785–796, https://doi.org/10.1038/nrd1494.

[43] E. Sjökvist, C. Nyström, M. Aldén, Physicochemical aspects of drug release. XIII. The effect of sodium dodecyl sulphate additions on the structure and dissolution of a drug in solid dispersions, Int. J. Pharm. 69 (1991) 53–62, https://doi.org/10.1016/0378-5173(91)90086-4.

[44] Y. Guo, C. Wang, J. Dun, L. Du, M. Hawley, C.C. Sun, Mechanism for the reduced dissolution of ritonavir tablets by sodium lauryl sulfate, J. Pharm. Sci. 108 (2019) 516–524, https://doi.org/10.1016/j.xphs.2018.10.047.

[45] S. Patil, S. Suryavanshi, S. Pathak, S. Sharma, V. Patravale, Evaluation of novel lipid based formulation of β-Artemether and Lumefantrine in murine malaria model, Int. J. Pharm. 455 (2013) 229–234, https://doi.org/10.1016/j.ijpharm.2013.07.033.

[46] B. Finnin, K.A. Walters, T.J. Franz, In vitro skin permeation methodology, Transdermal Top. Drug Deliv. Princ. Pract. (2012) 85–108, https://doi.org/10.1002/9781118140505.ch5.

[47] P. Prabhu, S. Suryavanshi, S. Pathak, A. Patra, S. Sharma, V. Patravale, Nanostructured lipid carriers of artemether–lumefantrine combination for intravenous therapy of cerebral malaria, Int. J. Pharm. 513 (2016) 504–517, https://doi.org/10.1016/j.ijpharm.2016.09.008.

[48] R. Fule, D. Dhamecha, M. Maniruzzaman, A. Khale, Development of hot melt co-formulated antimalarial solid dispersion system in fi xed dose form (ARLUMELT): evaluating amorphous state and in vivo performance, Int. J. Pharm. 496 (2015) 137–156, https://doi.org/10.1016/j.ijpharm.2015.09.069.

[49] J.N. Pawar, R.T. Shete, A.B. Gangurde, K.K. Moravkar, S.D. Javeer, D.R. Jaiswar, P. D. Amin, Development of amorphous dispersions of artemether with hydrophilic polymers via spray drying: physicochemical and in silico studies, Asian J. Pharm. Sci. (2016), https://doi.org/10.1016/j.ajps.2015.08.012.

[50] G. Zhou, J.C. Yang, In situ UHV-TEM investigation of the kinetics of initial stages of oxidation on the roughened Cu(1 1 0) surface, Surf. Sci. 559 (2004) 100–110, https://doi.org/10.1016/j.susc.2004.04.046.

[51] S. Bhattacharjee, DLS and zeta potential - what they are and what they are not? J. Control. Release 235 (2016) 337–351, https://doi.org/10.1016/j.jconrel.2016.06.017.

[52] D. Parashar, N.P. Aditya, R.S.R. Murthy, Development of artemether and lumefantrine co-loaded nanostructured lipid carriers: physicochemical characterization and in vivo antimalarial activity, Drug Deliv. 23 (2016) 123–129, https://doi.org/10.3109/10717544.2014.905883.

[53] A.D. Permana, I.A. Tekko, M.T.C. McCrudden, Q.K. Anjani, D. Ramadon, H. O. McCarthy, R.F. Donnelly, Solid lipid nanoparticle-based dissolving microneedles: a promising intradermal lymph targeting drug delivery system with potential for enhanced treatment of lymphatic filariasis, J. Control. Release 316 (2019) 34–52, https://doi.org/10.1016/j.jconrel.2019.10.004.

[54] M.T.C. Mc Crudden, E. Larrañeta, A. Clark, C. Jarrahian, A. Rein-Weston, S. Lachau-Durand, N. Niemeijer, P. Williams, C. Haeck, H.O. McCarthy, D. Zehrung, R.F. Donnelly, Design, formulation and evaluation of novel dissolving microarray patches containing a long-acting rilpivirine nanosuspension, J. Control. Release 292 (2018) 119–129, https://doi.org/10.1016/j.jconrel.2018.11.002.

[55] S.R. Mudshinge, A.B. Deore, S. Patil, C.M. Bhalgat, Nanoparticles: emerging carriers for drug delivery, Saudi Pharm. J. 19 (2011) 129–141, https://doi.org/10.1016/j.jsps.2011.04.001.

[56] D.L. Pavia, G.M. Lampman, G.S. Kriz Jr., Introduction to spectroscopy: a guide for students of organic chemistry, Introd. to Spectrosc, 2008, pp. 105–112.

[57] D.L.B. Robert, M. Silverstein, Francis X. Webster, David Kiemle, The Spectrometric Identification of Organic Compounds, 8 edition, Wiley, 2014.

[58] P.R.S. Laura Moroni, Cristina Gellini, F.L. Maurizio Muniz Miranda, E.S. Maria Luisa Foresti, Massimo Innocenti, Raman and infrared characterization of the vibrational properties of the antimalarial drug artemisinin, J. Raman Spectrosc. 39 (2008) 276–283, https://doi.org/10.1002/jrs.1880.

[59] W.J. Kim, Gyeong-Man, Andre Wutzler, Hans-Joachim Radusch, Goerg H. Michler, Paul Simon, Ralph A. Sperling, Parak, one-dimensional arrangement of gold nanoparticles by electrospinning, Chem. Mater. 17 (2005) 4949–4957, https://doi.org/10.1021/cm0508120.

[60] B.S. Gao, L. Chen, W. Chen, Thermal stability evaluation of B-artemether by DSC and ARC, Thermochim. Acta 569 (2013) 134–138, https://doi.org/10.1016/j.tca.2013.07.017.

[61] S.L. Shmeis, A. Rama, Zeren Wang, Krill, A mechanistic investigation of an amorphous pharmaceutical and its solid dispersions, part I: a comparative analysis by thermally stimulated depolarization current and differential scanning calorimetry, Pharm. Res. 21 (2004) 2025–2030, https://doi.org/10.1023/B:PHAM.00000.

[62] M.A.A. O'Neill, S. Gaisford, Application and use of isothermal calorimetry in pharmaceutical development, Int. J. Pharm. 417 (2011) 83–93, https://doi.org/10.1016/j.ijpharm.2011.01.038.

[63] P. González-Vázquez, E. Larrañeta, M.T.C. McCrudden, C. Jarrahian, A. Rein-Weston, M. Quintanar-Solares, D. Zehrung, H. McCarthy, A.J. Courtenay, R. F. Donnelly, Transdermal delivery of gentamicin using dissolving microneedle arrays for potential treatment of neonatal sepsis, J. Control. Release 265 (2017) 30–40, https://doi.org/10.1016/j.jconrel.2017.07.032.

[64] L.G.C. Burkhart, D. Morrell, Dermatological pharmacology, in: B.C.K.L.L. Brunton, A.B. Chabner (Eds.), Goodman Gilman's Farmacol. Basis Ther, 12a ed, McGraw-Hill Medical, New York, NY, 2012.

[65] Y. Qiu, C. Li, S. Zhang, G. Yang, M. He, Y. Gao, Systemic delivery of artemether by dissolving microneedles, Int. J. Pharm. 508 (2016) 1–9, https://doi.org/10.1016/j.ijpharm.2016.05.006.

[66] S. Salman, T.C. Bendel, Lee Daryl, T.M.E. Davis, D. Templeton, Pharmacokinetics of a novel sublingual spray formulation of the antimalarial drug artemether in African children with malaria, Antimicrob. Agents Chemother. 59 (2015) 3208–3215, https://doi.org/10.1128/aac.05014-14.

[67] J. Jain, J. Leong, L. Chen, S. Kalluri, V. Koradia, D. Stein, M. Wolf, G. Sunkara, J. Kotaa, Bioavailability of lumefantrine is significantly enhanced with a novel formulation approach, an outcome from a randomized, open-label pharmacokinetic study in healthy volunteers, Antimicrob. Agents Chemother. 61 (2017) 1–10.

[68] P.O. Nnamani, M. Windbergs, C. Lehr, Development of artemether-loaded nanostructured lipid carrier (NLC) formulation for topical application 477, 2014, pp. 208–217.

[69] I.C. César, J.A. de Aquino Ribeiro, L. de Souza Teixeira, K.B. Bellorio, F.C. de Abreu, J.M. Moreira, P.R. Chellini, G.A. Pianetti, Liquid chromatography-tandem mass spectrometry for the simultaneous quantitation of artemether and lumefantrine in human plasma: application for a pharmacokinetic study, J. Pharm. Biomed. Anal. (2011), https://doi.org/10.1016/j.jpba.2010.07.027.

[70] V.G. Dos Santos, R.J. Alves, M.N. Eberlin, G.A. Pianetti, I.C. César, A electrospray ionization tandem mass spectrometry of the two Main antimalarial drugs: artemether and lumefantrine, Artic. J. Braz. Chem. Soc. 23 (2012) 65–71.

[71] F.V. Zanutto, P.K. Boldrin, E.A. Varanda, S.F. De Souza, P.T. Sano, W. Vilegas, L. C. Dos Santos, Characterization of flavonoids and naphthopyranones in methanol extracts of Paepalanthus chiquitensis herzog by HPLC-ESI-IT-MS<inf>n</inf> and their mutagenic activity, Molecules 18 (2013), https://doi.org/10.3390/molecules18010244.

[72] WHO, World health organization model list of essential medicines, Ment. Holist. Heal. Some Int. Perspect, 2019, pp. 119–134. https://apps.who.int/iris/bitstream/handle/10665/325771/WHO-MVP-EMP-IAU-2019.06-eng.pdf?ua=1.

[73] W. World Health Organization, WHO Model List of Essential Medicines, 2017.

[74] F. Food and Drug Administration, Guidance for Industry: Estimating the Maximum Safe Starting Dose in Initial Clinical Trials for Therapeutics in Adult Healthy Volunteers, July (2005) 1–30, https://www.fda.gov/regulatory-information/search-fda-guidance-documents/estimating-maximum-safe-starting-dose-initial-clinical-trials-therapeutics-adult-healthy-volunteers, 2005 (accessed November 10, 2020).

[75] S. Reagan-Shaw, M. Nihal, N. Ahmad, Dose translation from animal to human studies revisited, FASEB J. 22 (2008) 659–661, https://doi.org/10.1096/fj.07-9574lsf.

[76] A. Djimdé, G. Lefèvre, Understanding the pharmacokinetics of Coartem ® 8, 2009, pp. 1–8, https://doi.org/10.1186/1475-2875-8-S1-S4.

[77] N.M. Anstey, R.N. Price, M.E.T. Davis, et al., The effect of dose on the antimalarial efficacy of artemether-lumefantrine: a systematic review and pooled analysis of individual patient data, Lancet Infect. Dis. 15 (2015) 692–702, https://doi.org/10.1016/S1473-3099(15)70024-1.

[78] M. Van Vugt, A. Brockman, B. Gemperli, C. Luxemburger, I. Gathmann, C. Royce, T. Slight, S. Looareesuwan, N.J. White, F. Nosten, Randomized comparison of artemether-benflumetol and artesunate- mefloquine in treatment of multidrug-resistant falciparum malaria, Antimicrob. Agents Chemother. 42 (1998) 135–139, https://doi.org/10.1128/aac.42.1.135.

[79] N.M. Anstey, R.N. Price, T.M.E. Davis, et al., The effect of dose on the antimalarial efficacy of artemether-lumefantrine: a systematic review and pooled analysis of

individual patient data, Lancet Infect. Dis. 15 (2015) 692–702, https://doi.org/10.1016/S1473-3099(15)70024-1.
[80] C. Nsanzabana, Resistance to Artemisinin combination therapies (ACTs): do not forget the partner drug!, Trop. Med. Infect. Dis. 4 (2019) 26, https://doi.org/10.3390/tropicalmed4010026.
[81] Y. Lubell, H. Reybur, H. Mbakilwa, et al., The cost-effectiveness of parasitologic diagnosis for malaria-suspected patients in an era of combination therapy, in: W.N. Breman JG, M.S. Alilio (Eds.), Defin. Defeating Intolerable Burd. Malar. III Prog. Perspect., American Society of Tropical Medicine and Hygiene, 2007.